INTEGRATION OF ENZYME-BASED BIOSENSORS AND CMOS ELECTROCHEMICAL INSTRUMENTATION THROUGH A LAB-ON-CMOS PLATFORM

By

Yue Huang

A DISSERTATION

Submitted to
Michigan State University
in partial fulfillment of the requirements
for the degree of

DOCTOR OF PHILSOPHY

Electrical Engineering

2011

ABSTRACT

INTEGRATION OF ENZYME-BASED BIOSENSORS AND CMOS ELECTROCHEMICAL INSTRUMENTATION THROUGH A LAB-ON-CMOS PLATFORM

By

Yue Huang

Redox enzyme based electrochemical biosensors provide label-free continuous monitoring of biomolecules. This thesis work aims to solve the key challenges in constructing a microsystem that integrates enzyme-based electrochemical sensors, electrode arrays, CMOS instrumentation circuits, and microfluidics. A CMOS compatible enzyme immobilization technique based on conductive polymers is introduced and demonstrated through a biosensor based on an alcohol dehydrogenase enzyme. Utilizing a thorough study of the cross-disciplinary compatibility requirements for on-CMOS electrochemical sensors, a microfabricated electrode array scheme is identified and further optimized through a concentric ring working electrode design that minimizes electrode area and processing complexity. A new CMOS bipotentiostat architecture is introduced which, when used in conjunction with the concentric ring electrodes, implements an electrochemical interrogation scheme that enables signal amplification through the redox recycling with enzyme modified electrodes. Finally, a novel lab-on-CMOS integration platform is introduced that unites the capabilities of lab-on-chip microfluidic systems with the performance advantages of CMOS microsystems to integrated bios. This work establishes a miniaturized platform for integrating a variety of enzymes as biosensing elements that can be utilized to analyze biological samples using powerful electrochemical techniques. By integrating significant developments in enzyme

immobilization, CMOS compatible microelectrode arrays, and CMOS instrumentation for redox recycling, this research advances the fields of point-of-care medical diagnostics, high-throughput screening, and a wide range of additional sensing applications.

ACKNOWLEDGEMENT

I would like to thank my advisors, Prof. Andrew Mason, for his invaluable mentorship, encouragement and inspiration. I feel so grateful and lucky to have the opportunities of free research, and the experience of grant applications and teaching under his supervision. Prof. Mason's support is not only as a mentor, but also as a good friend in life.

I would like to thank my committee members, Prof. Mark Worden, Prof. Shantanu Chakrabartty and Prof. Tim Hogan for their valuable advice and unconditional support during my study. I would also like to thank Prof. Xiangqun Zeng, Prof. Wen Li and Prof. Clare Vieille. Your help introduced me into a fascinating world of electronics, microfabrication, analytical chemistry and biochemistry that ultimately linked together.

I would like to thank my colleagues, Jichun Zhang, Junwei Zhou, Chao Yang, Daniel Rairigh, Xiaowen Liu, Lin Li, and many more whose name are not listed here, whom I developed friendships with that I will never forget. It remains one of my most valuable possessions that will prevail.

I would not thank my parents and family members, because words are not enough to express my appreciation and gratitude for their support, tolerance, encouragement and sacrifice.

TABLE OF CONTENTS

LIST OF TABLES

LIST OF FIGURES

NOMENCLATURE

C_{dl}	Double layer capacitance
D	Diffusion coefficient
F	Faraday constant
n	Number of electrons transferred
J	Current density
k_p	Partition coefficient
k_{cat}	Catalytic turnover number
K_m	Michaelis-menten constant
m_e	Rate of mass transfer in the bulk
P_m	Permeability inside the enzyme layer
R_{ct}	Charge transfer resistance
R_s	Resistance of solution
Z_w	Warburg-diffusion impedance

ABBREVIATIONS

AFM Atomic force microscopy

BLM Bilayer lipid membrane

CE Counter electrode

CMOS Complementary metal–oxide–semiconductor

CP Conductive polymer

CV Cyclic voltammetry

CVD Chemical vapor deposition

CYS Cystein

DTT Dithiothreitol

EIS Electrochemical impedance spectroscopy

EDS Energy dispersive spectroscopy

FAD Flavin adenine dinucleotide

HPLC High performance (pressure) liquid chromatography

IC Integrated circuit

IDA Interdigited array electrode

IR Current resistor product

MOSIS An Multi-project wafer (MPW) of integrated circuit fabrication service provider

MSA Molecular self-assembly

NAD β-nicotinamide adenine dinucleotide (NAD^+)

NADP β-nicotinamide adenine dinucleotide phosphate ($NADP^+$)

pAPBA Poly-aminophenylboronic acid

PBS Phosphate buffer solution

PDMS Poly(dimethylsiloxane)

PMMA Polymethyl-methacrylate

PPy Poly-pyrrole

PVD Physical vapor deposition

QCM Quartz crystal microbalance

RE Reference electrode

SAM Self-assembled monolayer

SEM Scanning electron microscopy

sADH Secondary alcohol dehydrogenase

sADH I86A Secondary alcohol dehydrogenase with isoleucine at 86^{th} codon replaced by alanine

tBLM Tethered bilayer lipid membrane

1 Introduction

1.1 Overview of Integrating Electrochemical Enzyme Biosensor on CMOS Potentiostat

The ability to identify and measure analyte concentrations is indispensable in chemical, biological and medical application areas, such as environmental monitoring, bio-product manufacturing, biohazard detection, clinical diagnosis, and drug discovery [1-4]. By utilizing antibody, antigen, aptamer, DNA and peptide etc., biosensors offer great diversity, sensitivity and specificity in their ability to hybridize, bind, transfer and interact with target biological analytes [5]. Biosensors based on soluble proteins and membrane proteins carry the same merits. Furthermore, some of proteins can provide continuous and label-free measurements which are critical but most of other sensor technologies cannot. Enzyme-based biosensors represent a sub-class having been applied in monitoring glucose, lactate, etc [4, 6, 7]. For example, glucose sensors, the first and the most successful biosensors, are typically constructed of electrochemical electrodes conditioned with glucose enzymes [6]. The industry has been seeking miniaturized enzyme-based systems that allow continuous monitoring of bio-molecule. Realization of such systems inevitably requires synergistic integration of enzyme, transducer, instrumentation and packaging.

Reagentless continuous operation of an enzyme-based electrochemical biosensor suggests enzymes, cofactors and mediators to be immobilized on an electrode [8]. Immobilization prevents enzymes from being consumed or washed away and maintains the interface. By immobilization an electron transfer pathway between the enzyme and

the electrode is built to supply the enzyme with electrons or protons for it to function continuously. In order to be immobilized, enzyme could be physically entrapped in polymer matrices or chemically bounded onto an electrode surface. By coupling enzymes to an electrode, molecular interactions between the enzymes and the target analyte can be directly converted into electrical signals that reflects the analyte concentration [9, 10].

The transducer of an enzyme-based electrochemical biosensor, the electrode, converts the collective response of enzymes into electrical signals. To be more specific, the enzyme-modified electrode is used as the working electrode of an electrochemical cell which often consists of a working electrode, a counter electrode, a reference electrode and electrolyte. An electrochemical transducer requires no labeling molecules and is relatively simple and easy to miniaturize than an optical transducer consisting of light source, lens, filter and light sensor [11, 12]. In addition miniaturization of electrochemical transducer can create microelectrodes that are favored in electrochemistry for its fast response, higher signal to noise ratio and other advantages [13].

The electrochemical instrumentation circuits can be implemented by the popular complementary metal–oxide–semiconductor (CMOS) microelectronics technology. As proper electrochemical technique is determined, CMOS application specific integrated circuits (ASIC) can be customized and optimized to interrogate an enzyme-based biosensor. A commonly used potentiostat is the instrument for performing amperometry to control the potential over a working electrode and records the current flowing through it. Microfabrication technology for making electrodes including thin film deposition and photolithography is a subset of the tools of the semiconductor industry for fabricating

CMOS integrated circuits (IC) [14]. A foundry is capable of producing the CMOS electrochemical instrumentation ICs and electrodes at low cost in mass production. Non-standard processes can be performed post CMOS for electrodes, enzyme immobilization and packaging.

Many fluidic handling lab-on-chip (LOC) devices have been realized with CMOS-compatible processes [15]. However, a distinct lack of integration of CMOS ICs and LOC remains as a major obstacle toward miniaturization of the entire instrumentation system, which is appealing for many applications including high throughput drug screening, medical point-of-care, and biological research. Bring together microsystems and LOCs onto a CMOS IC to be a lab-on-CMOS combines the power of all, significantly reduces footprint of the system, reduces the consumption and expenses of analyte and consumables and enhances the detection performance. A microelectrode array with incorporating microfluidic components can provide parallelism to improve throughput or redundancy to improve reliability in case of failures for fast simultaneous high-throughput measurements. Very few microsystems with electrochemical sensors and corresponding circuits have been realized [16-21]. Figure 1.1 illustrates a conceptual electrochemical biosensor array lab-on-CMOS based on a CMOS IC, with fluid delivery to the electrode array on top. To the best of our knowledge, an enzyme-based lab-on-CMOS has not been reported.

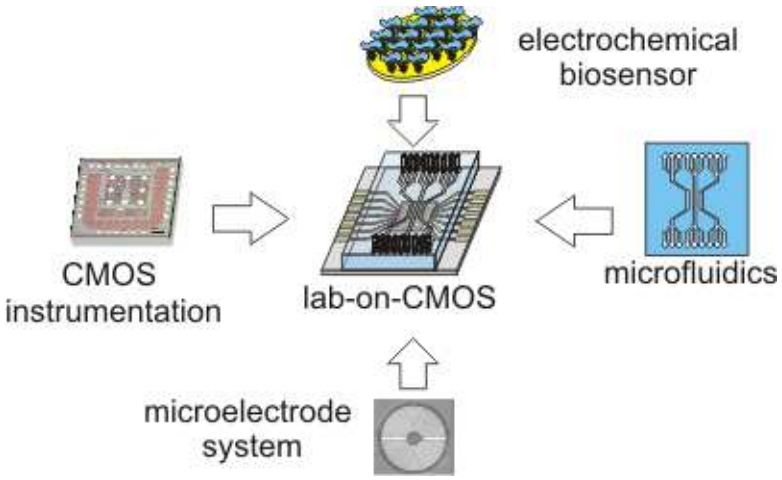

Figure 1.1: The conceptual lab-on-CMOS device consists of an electrochemical biosensor, an electrode array, a microfluidic sample handling device and a CMOS integrated electrochemical instrumentation circuit. (For interpretation of the references to color in this and all other figures, the reader is referred to the electronic version of this dissertation.)

1.2 Enzyme-based Electrochemical Biosensors

Electrochemical biosensors are critical reviewed by Wang [3], Grieshaber [22], Wang [23] and Ronkainen [24]. Among them, enzyme-based electrochemical biosensors are more suitable for implementing on a CMOS chip than affinity based biosensors because it functions continuously that merit the cost of CMOS. Enzymes are excellent molecular recognition elements for biosensors, offering great diversity, sensitivity and specificity. Enzymes are known to catalyze about 4,000 biochemical reactions. Compared to DNA, aptamer and antibody-antigen that rely on binding that are normally one-shot, some enzymes, *Oxidoreductase*, provide label-free, continuous detection when used as bio-recognition element. Comparison of bio-recognition elements with respect to their recognition mode, transducer types, labeling requirements and operation mode is shown in Table 1.1. An example glucose, lactate, and pyruvate enzyme biosensor array on a microfabricated gold electrode exhibited an opportunity of applying to intensive blood

glucose monitoring [4]. Other bio-molecules such as amino acid, steroid, alcohols can also be detected by enzyme biosensors. Table 1.2 lists compounds that can be detected by amperometric enzyme biosensors.

Bio-recognition element	Recognition mode	Transducer	Label Free	Continuous
DNA probe	Hydrogen bonds	Optical Electrochemical	N	N
Aptamer	Affinity	Optical	N	N
Antibody-Antigen	Affinity	Optical, Electrochemical	N	N
Enzyme	Reduction-oxidization	Optical Electrochemical	Y	Y

Table 1.1: Comparison of bio-recognition elements.

Class	Compounds
Carbohydrates	Glucose, Lactose, Maltose, Fructose, Xylose, Galactose, Sucrose, Cellobiose, Mannose, Arabinose
Amino acids	Aspartate, Sarcosine, N-Benzoyl-L-tyrosine, Glutamate, L-Phenylalanine
Carboxylic acids	Ascorbate, Pyruvate, Lactate, Malate, Oxalate, Glycolate, Tartarate, Fumarate
Alcohols and Phenols	Ethanol, Methanol, Cholesterol esters, Cholesterol, Bilirubin, Phenol, p-Cresol, Catechol, o-Aminophenol, o-Cresol, Dopamine
Amines and Heterocycles	Acetylcholine, Uric acid, Hypoxanthine, Choline, Xanthine, Histamine, Putrescine
Aldehyde	Formaldehyde
Inorganic ions	Nitrate, Sulfite, Oxygen, Potassium ion
Oxide and Peroxide	Nitric oxide, Hydrogen peroxide
Quinone	Vitamin K
Steroids	Testosterone, Estradiol, Bile acid
Azide	Sodium azide
Hemoprotein	Cytochrome c

Table 1.2: Substrates that can be detected by electrochemical enzyme biosensors.

To understand the mechanisms of enzyme operation, a “lock-and-key” hypothesis model is described in Figure 1.2. The active site of an enzyme is shaped like a pocket with geometry suitable for containing a specific group of molecules with the chemical group inside the pocket to attract, lock, convert and release the specific molecule. According to their functionality, enzymes are categorized into *Oxidoreductase*, *Transferases, Hydrolases, Lyases, Isomerases, Ligases. Oxidoreductase,* including oxidase, dehydrogenase and peroxidase associates with direct electron transfer, is suitable for constructing electrochemical biosensor [25].

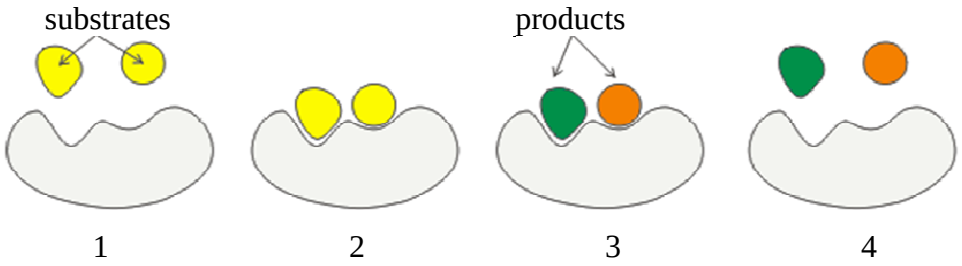

Figure 1.2: Diagrams to show the “lock-and-key” hypothesis of enzyme action. 1. Substrates entering enzyme active sites; 2. Substrates-enzyme complex; 3. Substrates-products complex; 4. Products leaving complex.

Enzymes lower the activation energy that a reaction requires. In free solution, a group of molecules, called cofactors or co-enzymes, help recover the enzymatic activity. There are three nature enzyme cofactors, NAD, NADP and FAD, each serving corresponding enzymes. In an organism, cofactors carry electrons to or from enzymes to recover the activity of enzymes, are recycled as a part of metabolism. In an enzyme-based biosensor the activation energy can be tuned to favor a reaction. Immediately, the enzymatic activity must be recovered for continuous operation.

To construct self-contained (autonomous) label-free biosensors with enzymes, enzymes and their cofactors are immobilized on an electrode surface. The activation

energy of individual enzyme and its catalytic reaction that involves electron transfer can be controlled by an excitation potential. As a collective of electron transfer activity, the resulting current is a function of the substrate concentration. For example, alcohol dehydrogenase (ADH, EC 1.1.1.1) is a group of seven dehydrogenase enzymes that occurs in many organisms and facilitates the interconversion between alcohols and aldehydes or ketones. In the human body, those enzymes break down alcohols which could otherwise be toxic. As a model for this research, secondary alcohol dehydrogenase (sADH), an *Oxidoreductase,* once drained electrons, catalyzes the reaction for oxidizing ethanol ($\mathbf{CH_3CH_2OH}$, substrate) to produce acetaldehyde ($\mathbf{CH_3COH}$, product) is:

$$\boldsymbol{CH_3CH_2OH \overset{sADH}{\longleftrightarrow} CH_3COH + 2H}$$

$$\boldsymbol{NAD + H \leftrightarrow NADH}$$

where nicotinamide adenine dinucleotide (NAD), a cofactor of ADH, is reduced as ethanol is oxidized. When a biosensor with NAD immobilized is positively biased to the point of oxidizing NADH, NAD is continuously recovered. Enzyme activity is also maintained by recycling process. The recycling process of immobilized ADH enzyme, along with cofactor and mediator, is illustrated in Figure 1.4. The mediator facilitates electron transfer, thus lowering the overpotential to drive the reaction and protecting the enzyme from being denatured. An alcohol sensor based on sADH can be realized by measuring the current of transferred electrons.

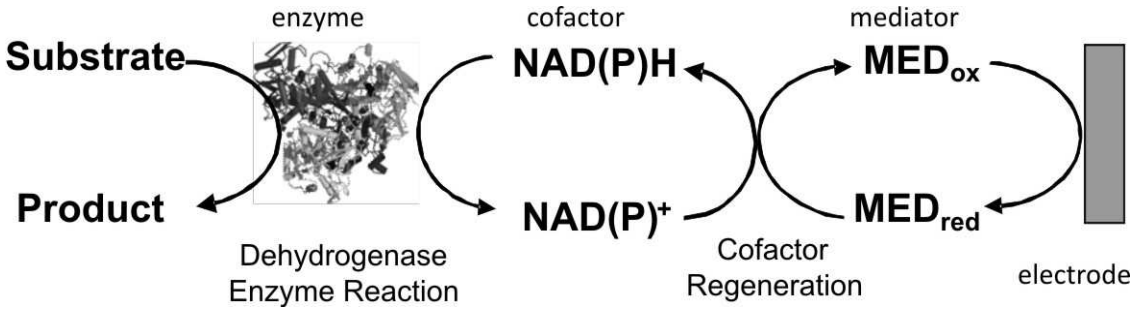

Figure 1.3: Immobilized enzyme along with cofactor and mediator. Recycling of cofactor and mediator maintains continuous enzyme activity.

1.3 Microfabricated Planar Microelectrode

As the transducer of an electrochemical biosensor, the electrode transforms chemical processes at the electrode surface into electrical signals for equipment to interpret. Such an electrode where interested reaction takes place is called a working electrode. A working electrode gains its sensing specificity through surface modification. Coupling an enzyme such as *Oxidoreductase* onto the electrode, molecular interactions between the enzyme and the target molecules can be converted directly into electrical signals, as explained in Section 1.2.

A typical electrode system consists of a working electrode, a counter electrode and a reference electrode. The performance of an electrode system can be greatly affected by its geometry [26]. A planar electrode system is adopted to integrate electrode system on the surface of a CMOS potentiostat, microfabrication technology, the same technology for fabricating CMOS chips, is used for making microelectrodes. The electrode geometrical factors of a planar electrode system involve considerations of microfabrication capability, electrochemical effects, enzyme activity, circuit layout, chip

size and surface profile, electrode materials, enzyme immobilization method, packaging and microfluidics.

Reference electrodes play a crucial role in an electrochemical system. It establishes a constant potential standard in measuring and controlling the working electrode potential, without being interfered by electrolyte solution. To match the geometrical requirements of planar microelectrode system, traditional reference electrode is not suitable. Miniaturized reference electrodes can be constructed by microfabrication. Microfabricated reference electrode in biosensing applications is reviewed by Sinwari, *et.al.* [27].

1.4 CMOS Electrochemical Instrumentation

An electrochemical instrument is a control and measurement device that keeps the potential of the working electrode at the desired level with respect to the reference electrode. At the same time, it records the current flowing between the working electrode and the counter electrode. Such an instrument is normally referred to as a potentiostat. A modern bench-top potentiostat is built with general purpose discrete electronic devices, including a microprocessor to communicate with computer-based software.

The electrochemical techniques that a potentiostat can perform include potentiometry, coulometry, voltammetry and impedance spectroscopy. Potentiometry measures the potential between two electrodes in a solution, which is related to the concentration of the analyte. A selective indicator electrode and a stable reference electrode are required for potentiometry. Coulometry uses applied current or potential to completely convert an analyte. By integrating the passing current, the number of

electrons indicates the amount of analyte. Coulometry is good for a small known volume of analyte or titration. Voltammetry measures the potential of an indicator electrode versus a reference electrode. Amperometry applies a constant and/or varying potential at an electrode's surface and measures the resulting current. This method can reveal the oxidation and reduction potential of an analyte and its reactivity that relates to the analyte concentration. Basics of electrochemical instrumentation and techniques are introduced in reference [26] and [28].

Electrochemical techniques that require complex data analysis and interpretation challenge the data processing capability, battery life and cost of a portable device. For a lab-on-CMOS, simple potential control and sensor data output is highly desired. For a particular electrochemical sensor, a suitable technique to extract the sensory response may be found. Once a sensor is characterized, redundant potentiostat functions of a general potentiostat can be removed to optimize the CMOS potentiostat.

1.5 Challenges in Integration of Electrochemical Enzyme Biosensors and CMOS Potentiostats

1.5.1 Overview

Figure 1.1 illustrates an example lab-on-CMOS platform integrating an enzyme-based biosensor onto a CMOS potentiostat. The device consists of electrochemical biosensors, electrode array, microfluidic sample handling structure and a CMOS integrated electrochemical instrumentation circuit. Some challenges are critical yet not stressed in literature. These includes the CMOS-bioelectronics interface, the microelectrode array and the post-CMOS microfabrication on CMOS, the

implementation of a CMOS electrochemical instrument and the packaging of an integrated circuit die for CMOS-microfluidics integration.

1.5.2 Enzyme Immobilization on CMOS

Basic requirements for enzyme immobilization are not only to physically attach enzyme to the electrode surface but also to create an electron transfer pathway and that maintains enzymatic activity. Furthermore, enzyme coverage should be uniform across the electrode, and the process should be suitable for batch fabrication. Two immobilization methods, molecular self-assembly (MSA) and conductive polymer co-immobilization are evaluated in this thesis research.

Many MSA heavily depends on thiol-metal bonding to bind the initial molecule layers onto an electrode. Noble metals are used because of the strong affinity of sulfur head groups for these metals. With self-assembly method, a mono-layer of enzyme is formed on metal electrode surface, providing uniform enzyme coverage from batch to batch. One challenge for this method is to facilitate electron transfer between enzymes and the electrode. Since the bonding molecules are not conductive, electron transfer is sluggish unless the electrons can acquire extra energy to hop across molecule layers or facilitated by an electron transfer mediator. The challenge in using MSA on a CMOS electrode array is to avoid fouling of counter electrode and reference electrode by MSA molecules, which reduces the CE and RE performance.

An alternative immobilization approach is to use electropolymerized conductive polymers. A challenge is to control the enzyme coverage uniformity that affects time response and sensitivity of the sensor. The conductive polymer and the embedded

enzyme could be selectively immobilized on the working electrode only. The tradeoff is that electropolymerization requires applying electric potential on the working electrode for the polymerization to happen; however it is not difficult if the working electrode is tied to a potentiostat as it would be in the lab-on-CMOS platform. This thesis work evaluates the MSA method and identifies an alternative method suitable for immobilizing enzyme on CMOS.

1.5.3 Microelectrode and Post-CMOS Microfabrication

Before fabricating microelectrodes on a CMOS chip, the electrode geometrical factors of planar electrodes must be determined. These geometrical factors include shape, size, spacing, and location. The design limitations factors of a planar electrode system involve microfabrication etc. as introduced in Section 1.3. Designing the microelectrode is a system level decision making problem that requires all of the above factors be taken into account.

Post-CMOS microfabrication of the electrodes on CMOS dice introduces practical challenges in photolithography and interconnection between electrodes and CMOS. Firstly, during photolithography, when photoresist is spin-coated on the chip during photolithography, the non-uniform buildup at chip edges or conglomeration in the chip center of photoresist greatly affects the quality of photolithography. Secondly, the sidewall of the contact openings in the passivation dielectric is steep which can break down the interconnection between the chip and the electrode. Thirdly, since the chip's final passivation dielectric layer is not planarized, the CMOS layout and the electrode location needs to be carefully planned to maintain smooth electrode surface.

Reference electrode plays an important role in voltammetry and amperometry. However, for a lab-on-CMOS platform, construction of a solid-state planar reference or pseudo reference electrode is limited by CMOS or CMOS compatible processes. These electrodes should be bio-compatible, not affected by bio-interface formation, and show low drift in the test environment. Finally, the reference electrode fabrication formation process must be scalable to fabricate on a CMOS die.

1.5.4 CMOS Potentiostat for Enzyme-based Biosensor Array

The first challenge is to determine a proper electrochemical technique that can extract the enzymatic sensory response in direct relation with substrate concentration and could easily be implemented to a CMOS potentiostat. For example, cyclic voltammetry (CV) is a good electrochemical technique for analytical purposes that could complicate the system. The species and concentration can be obtained from CV by the peak currents and the potentials at the peaks. To implement CV on a self-contained CMOS IC, triangle wave signal generator circuit should be designed for output the excitation signal, data digitization and storage should be available for storing data for using a microprocessor to extract the peak information. An open challenge is to identify more suitable electrochemical techniques for enzyme biosensor that could be effectively implemented in a simple CMOS.

The following challenge is to architect a potentiostat to support the determined electrochemical technique. For example, to take the advantage of redox recycling by applying amperometry on a pair of working electrodes could be manipulated by bipotentiostat architecture. Further, the ideal potentiostat architecture should support

electrode array for simultaneously readout. An architecture that is expandable to an array is appealing to replace the traditional adder potentiostat structure.

1.5.5 Lab-on-CMOS Packaging

The major challenge is to enable a CMOS chip to work in a liquid environment and to allow a high density microfluidic structure to access the on-chip electrode array. CMOS chip packaging process should free the chip from risk of ion contamination. Microfluidic structures are relatively larger than CMOS chips thus demand surface expansion for functional fluidic structures and interconnections. Microfluidic structures need a flat surface to bond to and reside on. Surface leveling is required for fluidic and electrical connections.

The packaging material for Lab-on-CMOS should be biocompatible, chemically inert and electrically insulating. Biocompatible materials are identified by ISO 10993, the international standard set for evaluating the biocompatibility of a medical device. The device should be reliable and endurable for working in harsh chemical environment during enzyme immobilization and testing, without adversely affecting the enzyme activity and test environment. Inter-compatibility of materials used in processes and bonding of interfacial materials are major fabrication challenges.

The packaging materials and process should also be determined by CMOS compatibility. Process of higher than 400 ˚C may cause failure of aluminum traces. The packaging material should not require processing above 400 ˚C. Certain metal ions diffuse quickly in silicon. The bulk silicon should be properly protected from contacting

aqueous solution during processes to avoid detrimental effects on threshold voltage chronically.

1.6 Research Goal

The goal of this research is to establish a Lab-on-CMOS methodology to highlight the power of integrating microelectronics and biosensors by demonstrating an incorporation of enzyme biosensors onto electrode arrays formed CMOS instrumentation and combines with microfluidics. This goal will be achieved through analysis, judicious selection and optimization of appropriate technologies. To achieve this goal, efforts in enzyme immobilization, planar electrode system and fabrication, and CMOS potentiostat instrumentation are reported in Chapter 2, 3 and 4, respectively. Chapter 5 introduces a Lab-on-CMOS scheme that allows integration of CMOS with microfluidic structure.

2 Electrochemical Enzymatic Bioelectronic Interface

2.1 Overview

This research seeks solutions of integrating enzyme-based biosensors on CMOS. Enzyme-based biosensors were introduced in Section 1.2. The challenges for building up enzymatic bioelectronic interface on CMOS are discussed in Section 1.5.2. In this chapter, two enzyme immobilization schemes are introduced. One scheme uses MSA to bind mono layers of linking molecules, cofactors, electron mediators and enzymes onto to a gold electrode. The other scheme we invented combines conductive polymer and molecular self-assembly, referred to hereafter CP-MSA. The CP-MSA method uses conductive polymers as initial layers, eliminating the dependence of gold, and then binds the cofactors and enzymes by molecular self-assembly as the MSA scheme.

2.2 Background

For enzyme biosensors based on oxidase enzymes, the substrate concentration is indirectly deduced by detecting the byproduct, hydrogen peroxide, produced during the catalyzed oxidation reaction and diffused onto the detector electrode. One of the inherent drawbacks is the oxygen concentration dependency. Its non-oxygen-dependant substituent, dehydrogenases normally require specific cofactors. To improve the poor electron transfer efficiency from cofactors to electrode surface, electron mediators are added to the free solution as electron-carrying vehicles to improve mass transport. By adding mediators, the destructive high over-potential applied to the protein interface is mitigated. Instead of contained in solution, electron mediators have been co-immobilized along with the enzymes and the corresponding cofactors [7]. By constructing a direct

electron transfer pathway from enzyme to electrode, no mediator in free solution is involved, thus increasing the sensory current and minimizing the side-effects of mediators. As an extension of this work, researchers are currently trying to simplify the process by engineering mutant enzymes that embed the functions of both cofactors and mediators.

Enzyme immobilization methodology for electrochemical sensors follows some criteria. First, the active sites of enzyme should be accessible by substrate after immobilization. Second, the enzyme has to maintain functionality without being denatured. Third, a facilitated electron pathway is crucial for the sensitivity and stability of the sensor.

There are many immobilization techniques available, such as adsorption, encapsulation, entrapment, cross-linking, and covalent bonding. MSA method by covalent bonding and conductive polymer entrapment method are suitable methods for application on a CMOS microelectrode because they allow non-manual immobilization on small electrode footprints and are individually addressable. The immobilization methods using self-assembled molecules and polymer matrices were critically reviewed [2,8][29].

The target enzyme, *Oxidoreductase,* including oxidase and dehydrogenase, requires cofactors or electron mediators to restore its activity. In nature, there are only a few types of cofactors for the above enzymes. It allows researchers to develop a sensor platform by immobilizing those cofactors and thus corresponding enzymes. Numerous biosensors can be built based on such platform by exchanging only the enzymes to detect

correspondent biomolecues. This platform is promising in building an array of biosensors for detecting several bio-molecules in biological relevance.

The objective of research in this chapter is to determine suitable technologies for immobilizing enzyme on post-CMOS microelectrodes. With the microsystem constraint in mind, immobilization of dehydrogenase enzymes using MSA is evaluated and a new immobilization scheme using conductive polymers and MSA to overcome fabrication limitations of MSA method is introduced.

2.3 Immobilization of Enzyme by Molecular Self-assembly

2.3.1 Background

Enzymes that are dependent on cofactors (NAD, $NAD(P)^+$ or FAD) have been immobilized on gold electrode by several MSA schemes [9]. The collaborators in Prof. Worden's lab have developed a novel immobilization method using a hetero-functional linker molecule [10]. The structure is shown in Figure 2.1. It uses cysteine, a branched amino acid having sulfhydryl, amino, and carboxyl functional groups, as a linker. The sulfhydryl group of cysteine provides thiol-Au bonding to anchor itself on gold electrode surface. Cysteine also links to the electron mediator toluidine blue O (TBO) through the carboxyl group, and to the cofactor (e.g. $NAD(P)^+$) through the amino group. This structure is comparable with previously reported approaches that bind the enzyme, cofactor, and mediator in a linear chain.

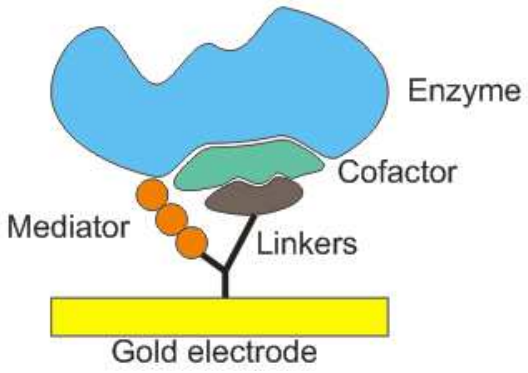

Figure 2.1: Enzyme immobilized by molecular self-assembly on gold electrode by using a hetero-functional linker molecule.

2.3.2 Experiment

A 2mm diameter gold disk electrode was fabricated using CMOS compatible processes by physical vapor deposition of 5nm Ti/100nm Au on dielectric substrate followed by photolithography and lifting off. The processes are discussed in details in Chapter 3. An alcohol sensor was developed on the gold electrode by immobilizing site-mutated secondary alcohol dehydrogenase (sADH I86A) using the MSA method described in Section 2.3.1. The modified electrode was connected to a CHI 660 Electrochemical Workstation as the working electrode. Cyclic voltammetry (CV) was performed to examine the sensor's response. The potential swept from -200 mV to 400 mV at a scanning rate of 100 mV s^{-1}. A series concentration of several representative aryl and chiral alcohols in 10X Phosphate Buffer Solution (PBS) was tested.

2.3.3 Results and Discussion

The cyclic voltammogram in Figure 2.2 showed reduction peaks and the oxidation peaks at 160mV (vs. Ag/AgCl reference electrode) and 200 mV respectively. The

magnitude of peaks was found to increase with ethanol concentration in the tested range from 5mM to 25mM.

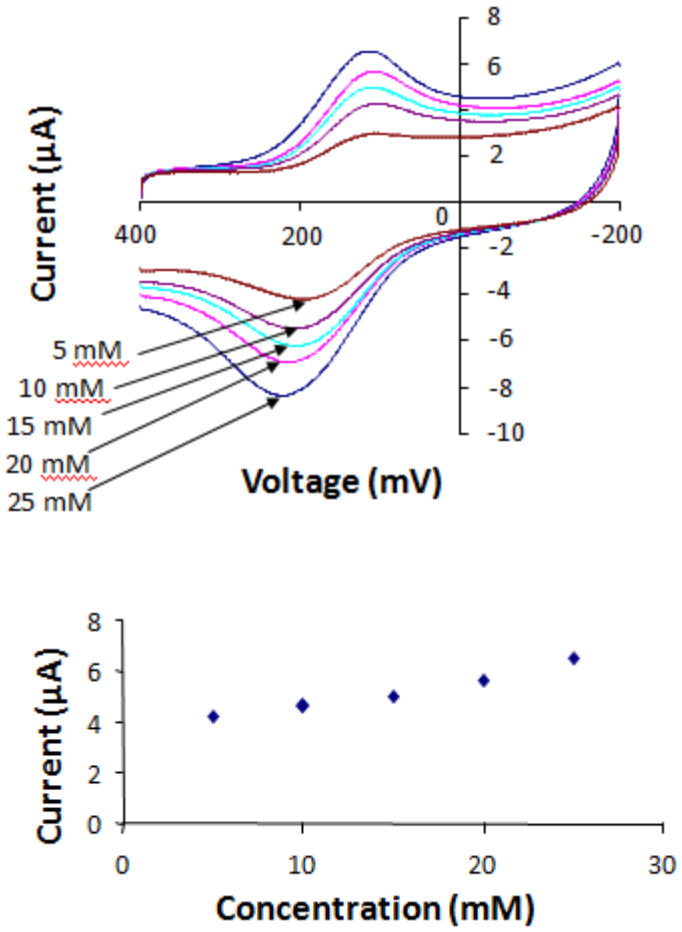

Figure 2.2: CV plot and the calibration curve of various concentration of ethanol on sADH I86A mutant enzyme immobilized electrode.

CV experiments were also performed on the sensor in isopropanol, butanol and acetophenone substrates. Table 2.1 compares the saturation current and the sensitivity of both wild-type and mutant enzyme in those substrates respectively.

Experimental results show a functioning enzyme-based alcohol biosensor. The experiment suggests MSA method can be utilized to create an electrochemical enzymatic

sensor interface on microfabricated gold electrode. This method relies on gold or other noble metals for the initial molecular bindings that require post-CMOS fabrication process on a foundry CMOS chip.

Substrate	Sensitivity ($\mu AmM^{-1}cm^{-2}$)
Ethanol	0.71
Isopropanol	1.16
Butanol	0.29
Acetophenone	1.89

Table 2.1: The sensitivity results from the cyclic voltammograms for the CYS-TBO-$NADP^+$-sADH I86A functionalized gold electrode in the presence of different concentrations of alcohols or ketones. Acetophenone is 25% w:v acetonitrile in PBS.

2.4 Immobilization of Enzyme by Conductive Polymer

2.4.1 Background

An alternative enzyme immobilization technique for CMOS electrode is using conductive polymer (CP), that is compatible with silicon technology [30]. Since MSA method requires gold electrode surface, to form such an interface onto a CMOS chip, fabrication steps in addition to standard CMOS processes are required to deposit and pattern gold working electrodes. Furthermore, to avoid the counter electrode being fouled by MSA thiol linking molecules, additional masking processes or surface pretreatment of

the counter electrode is needed. Otherwise, the effective area of counter electrode would be greatly reduced by fouling. In contrast, CP can be selectively synthesized on working electrode without fouling other electrodes. Besides, CP can be formed on CMOS aluminum [31]. If it is true that enzyme immobilization can be achieved on CMOS aluminum, compared to the MSA method, CP method will have the advantage in processing time, materials cost and electrode immobilization selectivity. The trade-off for these advantages is the added complexity of applying an external potential on the target electrode during polymerization.

Immobilization of biomolecules, including enzymes using CPs was reviewed by Schuhmann [30], Wallace [32], Gerard [33], Ahuja [34], Cosnier [29], *et. al*. The existing methods are co-entrapment of enzymes in conductive polymer matrices and adsorption of amphiphilic monomers and biomolecules [29]. Co-entrapment method produces a conductive polymer doped with multiple layers of enzymes. Such as a multilayer sensor based on the sequential electrochemical polymerization of pyrrole or pyrrole derivatives [35]. It generates a larger sensory current than the sensor with a monolayer of enzyme using MSA method, partly because of larger enzyme coverage per unit area. However, with the co-entrapment method, a greater portion of immobilized enzymes are buried in the conductive polymer matrices, retarding the sensor response. Response time becomes more critical as the scale of sensor array increases with fixed instrumentation circuits. Another disadvantage of co-entrapment is the lack of control in enzyme coverage uniformity, which is necessary to reduce sensor-to-sensor difference. Immobilization with enzyme monolayer avoids those drawbacks. A biotinylated glucose oxidase monolayer was immobilized through an avidin bridge [36]. Conductive polymer

polypyrrole was used for covalent binding to glucose oxidase to improve sensor response time [37]. Direct electron transfer was shown possible between vapor phase polymerized CP and GOx [38].

2.4.2 Design

In MSA method, phenylboronic acid is used to link FAD, NAD^+ or $NAD(P)^+$ by the double hydroxyl groups of the boronic acid. The challenge is the linking molecules are not conducting electrons, so electron mediator is needed. If a conductive media were bind to electrodes and enzymes, electron mediators may be saved. A candidate is a phenylboronic acid with amino group that can be electropolymerized, the precursor of poly-aminophenylboronic acid, both shown in Figure 2.3. The double hydroxyl group is not evolved in polymerization, suggesting that they are available to link enzyme cofactors.

Instead of entrapping multiple layers of enzymes in conductive polymer, a monolayer of enzymes can be immobilized through its corresponding cofactor as by the MSA method. This hybrid CP-MSA method can overcome the limitations in their applications to CMOS. This enzyme immobilization approach has not been reported by other researchers.

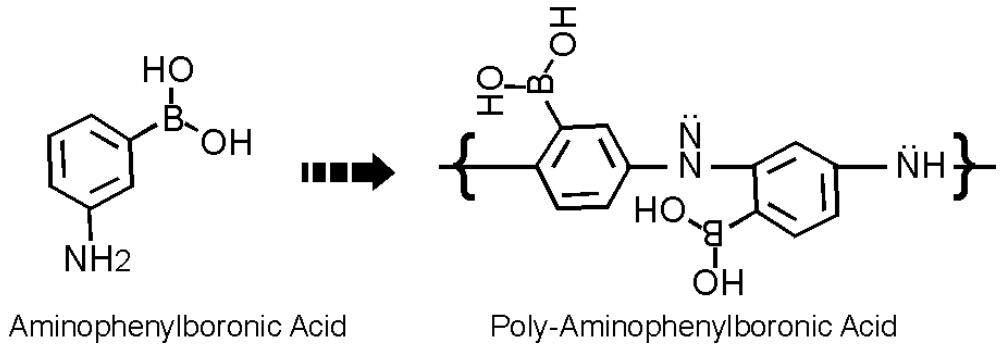

Figure 2.3: Molecular structure of aminophenylboronic acid and its polymerized form.

However, the poly-aminophenylboronic acid polymer shows poor adhesion to metal electrode surface. To promote the adhesion, an initial layer of conductive polymer, poly-pyrrole (PPy), was applied [39]. CMOS top metal layer, normally aluminum, is an active metal. By adding tartaric acid or saccharine, PPy was successfully formed on aluminum without corrosion [40, 41].

This new design features a PPy-pAPBA conductive polymer bi-layer, self-assembled enzyme cofactor by the double hydroxyl groups on pAPBA surface and attached cofactor dependant enzymes, as shown in Figure 2.4.

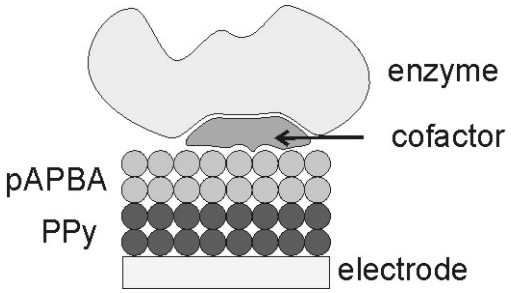

Figure 2.4: Enzyme immobilized onto conductive polymer through self-assembled cofactor.

2.4.3 Experiment

To validate the CP-MSA enzyme immobilization idea, two conductive polymer layers were electropolymerized on gold electrode surface, followed by bonding NAD cofactor and sADH enzyme. Each formation step was characterized. The formed alcohol sensor was tested using cyclic voltammetry.

Gold electrodes were prepared by photolithography and physical vapor deposition on glass substrate, as shown in Figure 2.5. Before electropolymerization, to remove absorbed organic contaminants the electrodes were cleaned using isopropyl and rinsed by DI water. To remove the native gold oxide on the electrodes, they were soaked in 0.1M HCl for 10 minutes, rinsed with DI water and dried with nitrogen. To electropolymerize pyrrole, a 100mM pyrrole solution was prepared in 10X PBS pH 7.4. The solution was homogenized and degassed before using. The electrode, along with an Ag/AgCl reference electrode and a gold counter electrode was then connected to an Omni-101 potentiostat. Two cycles of potential sweep from 0mV to 600mV at 100mV s^{-1} deposited a thin layer of PPy on the electrode. The cyclic voltammogram showed a sharp increasing oxidation current at over 400 mV, indicating the formation of polypyrrole. The electrode was rinsed and transferred to 1 mM 3-aminophenyleboronic acid solution. To deposited a thin layer of pAPBA on top of PPy, two cycles of potential sweep from 0 mV to 800 mV at 100 mV s^{-1} were performed.

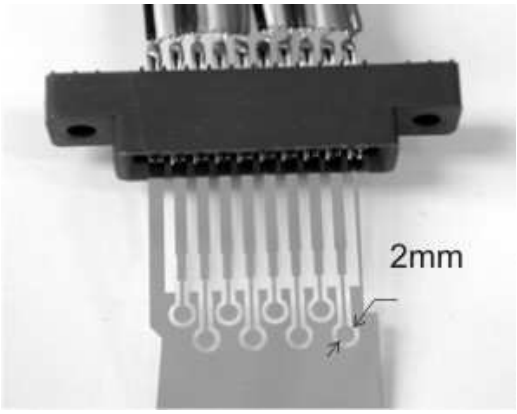

Figure 2.5: A microfabricated 8-electrode array for enzyme immobilization experiments.

Raman spectroscopy was used to examine the formation of conductive polymer layers by the signature spectrum of their chemical bonds. To confirm the formation of PPy, over-oxidized PPy on roughened gold electrode was examined before and after the formation of pAPBA. Figure 2.6 shows both of the labeled spectrums. The peaks of the PPy spectrum are the signature peaks of benzyl ring, amino group, etc., confirming the formation of PPy. The peak at wave number 1590 represents C-C in the benzyl ring, while the peak at wave number 1049 represents C=C. The ratio of the height of the two indicates the degree of oxidation. Because PPy and pAPBA are sharing similar molecular structures, the spectrum of pAPBA and PPy are alike, albeit the intensity at wave number 1590 and wave number 1049 differs. The higher ratio at wave number 1590 over wave number 1049 is due to the higher maximum potential, 800 mV, applied for polymerizing APBA. At this potential, the already polymerized PPy was further oxidized to a higher oxidation state. The reflected PPy light from underneath the pAPBA adds to that of pAPBA. The subtle differences are the small peaks between wave number from 600 to

800, which fall into the spectrum range of B-OH bonding that clearly differentiate PPy and pAPBA. These results confirm the formation of a layer of a pAPBA on PPy.

This hybrid method takes advantage of both conductive polymer and self-assembly. Without relying on gold surface, it provides greater flexibility for choosing electrode material including CMOS aluminum and cheap carbon ink printed electrodes. For immobilizing enzyme on the CMOS chip electrode surface, gold deposition and electrode patterning steps are saved. Compared to the self-assembly method, it spends less steps, processing time and chemicals.

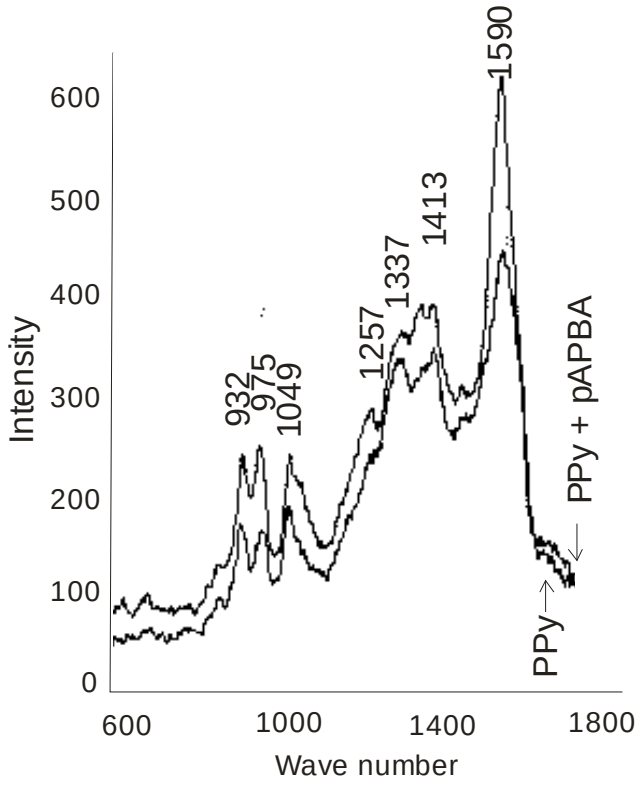

Figure 2.6: Raman spectrum of PPy and PPy-pAPBA formed on roughened gold electrode.

After electropolymerization of pAPBA, the NAD cofactor and sADH were self-assembled following published protocol for the MSA methods [10]. Briefly, the PPy-pAPBA electrode w soaked in 1 mM NAD solution for one hour and rinsed thoroughly to bind NAD. The PPy-pAPBA-NAD electrode was incubated in sADH I86A solution (6.8 mg/ml) for one hour and rinsed in running DI water to remove the loosely attached enzymes.

2.4.4 Results and Discussion

To verify that the enzymes were immobilized on the electrode and remained active, the PPy-pAPBA-NAD-sADH I86A modified electrode was tested using cyclic voltammetry in substrate solutions for the sensory response. It was tested in isopropyl solutions of various concentrations. Figure 2.7 shows the cyclic voltammogram. By recording the oxidation current at 300 mV, the sensitivity 1.30 $nAmM^{-1}cm^{-2}$ was observed from the calibration curve. Unlike the MSA method, there is no distinctive peak present in the cyclic voltammogram. It matches Zayats' experimental results. In Zayats' model on electron transfer, the exponential curves were explained as a result of electrons hopping over a band gap. Thus it is possible that because of the good wiring provided by CP, no electron hopping presented in the electron transport path, so there were no peaks in the cyclic voltammogram. However, comparing with the MSA method, the current is smaller, which may be caused by lack of immobilized enzyme being immobilized, or because the substrate was continuously consumed by the enzyme without pre-concentrating by electric force. Moreover, the maximum current is not limited by the hopping of the electron over a driving potential. Without having to drive the electrons to hop, the potential to drive the sensor can be reduced. Lowering working potential is

beneficial for reducing interference by other substances that are transformed at higher potential and contribute to the background current.

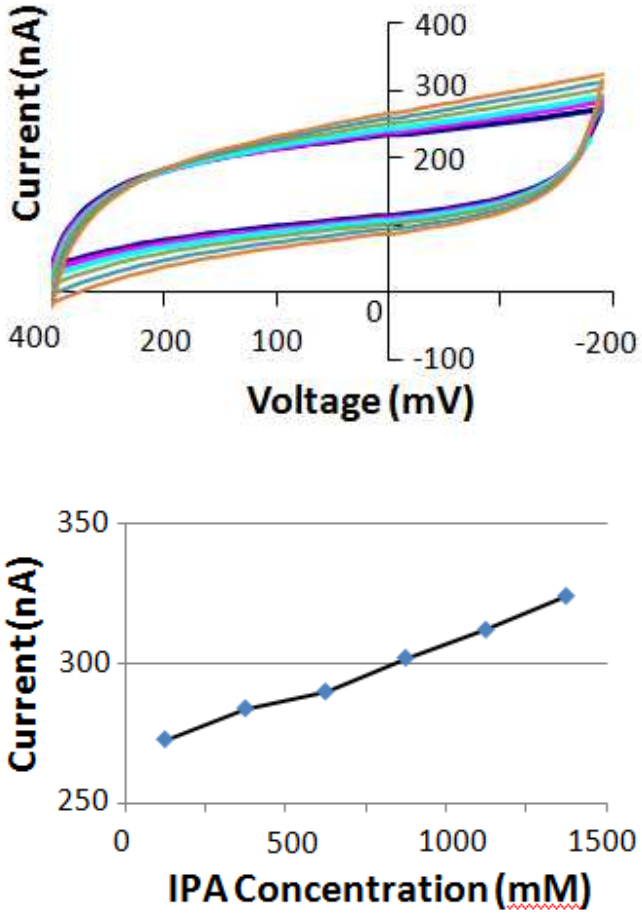

Figure 2.7: Cyclicvoltamogram (top) and calibration curve (bottom) of PPy-pAPBA-NAD-sADH I86A modified electrode tested in isopropyl alcohol concentration of ranging from 0 to 1250 mM.

2.5 Conclusion

A monolayer of enzyme was formed on microfabricated electrodes by both MSA and CP-MSA methods. Experimental results suggest both methods can be utilized to create an electrochemical enzymatic bioelectronic sensor interface. The CP-MSA method

developed by this thesis work does not require a gold electrode surface as its counterpart does and therefore it is directly compatible with CMOS process. CP-MSA is selective and does not foul the counter electrode. In addition, it saves not only expensive gold material, but also at least 50% of the processing time. Table 2.2 summarizes the performance of these two methods. The CP-MSA biosensor is favored from fabrication point of view, but could benefit from sensitivity improvement.

Immoblization Methods	Alcohol Sensor Sensitivity $nAmM^{-1}cm^{-2}$	CMOS Compatibility	Process Time
MSA	1160	post-CMOS	<12hrs
CP-MSA	1.30	Direct CMOS	<6hrs

Table 2.1 Comparison of sensitivity, CMOS compatibity and process time of MSA and CP-MSA methods applied to form an alcohol sensor.

3 Planar Electrode System and Microfabrication

3.1 Overview

To integrate an electrochemical electrode system on surface of a CMOS chip using foundry compatible microfabrication techniques, three electrodes system is designed in a planar fashion. Section 1.3 introduces the role of working electrode, planar electrode system performance and its geometry factors and design considerations. The challenges for realizing a planar electrode system on CMOS exist in design and fabrication, discussed in Section 1.5.3. In this research, issues involved electrode design and fabrication is discussed in detail. For electrode on chip, chip surface profile, circuit layout and microfabrication are also considered. The minimum size of the microelectrode is also limited by the enzyme activity after immobilization. In respect of material, noble metals such as gold are required for seeding the self-assembled bio-interface on the working electrode. The noble metal counter electrode could be formed the same time. But, the more complicated reference electrode requires additional processes, and remains stable in test environment.

In this chapter, planar electrode system and microfabrication background and analysis are given in Section 3.2 and Section 3.3. Prototyping planar microelectrode array and improvement on reference electrode are discussed in Section 3.4 and Section 3.5.

3.2 Background

Microfabrication has been used for many applications in medicine and biology to enhance the functions of conventional devices, such as tools for molecular biology and

biochemistry, tools for cell biology, medical devices, and biosensors [42]. Electrochemical sensors and microsystems were thoroughly reviewed in terms of techniques and performance along with the issues by Suzuki [43]. Microfabrication of a post-CMOS microelectrode system is an interdisciplinary problem spanning materials, microfabrication and electrochemistry. To date, fabrication of microelectrodes on a CMOS chip for enzyme-based electrochemical biosensors has not been reported. The electrode geometrical factors of planar electrodes have to be determined before fabrication. The design of an electrode system is complicated with electrochemical effects, electrode materials, immobilization of enzymes, enzyme activities, CMOS circuits and the microfabrication capabilities within the limitation of the small chip surface area.

The geometries on microelectrode size, shape, gap and positioning were studied by Bard [26], Whiteman [13] *et. al.* Few researches have constructed on-CMOS microelectrodes. Kovacs *et.al.* has designed an electrode array for mercury anodic stripping voltammetry [21]. Levine *et.al.* created a stepped-electrode process to simplify fabrication [17]. Thewes's group designed an CMOS gold interdigitated electrode array for redox recycling of probe molecules on immobilized DNA probe [16]. A microelectrode array was fabricated using CMOS process and electrolessplating [44]. To date, the geometry of on-CMOS electrode design has not been fully discussed. Research on planar microelectrodes for redox enzyme-based biosensors on CMOS has not been reported yet.

A crucial part of an electrochemical cell is reference electrode. Microfabricated planar reference electrode is a limitation of electrode performance. Research on

miniaturization of reference electrode and analysis of the parameters affecting its performance, stability and lifetime, is sparse. The requirements for reference electrodes are summarized in [27].

3.3 Analysis of Design Requirements

Well-established analytical electrochemical methods, such as cyclic voltammetry and electrochemical impedance spectroscopy can be used to analyze the analyte concentration. Although these methods are typically performed by using bench-top instruments, the biosensor microsystem introduced in the previous section is advantageous in many aspects. As the transducer for the integrated biosensing interfaces, the electrodes are firstly to be built onto the silicon chip surface, targeting on building a planar ultra-microelectrode array on the top of a CMOS chip. The involved issues include electrode configuration, geometry, material, and reliability etc. In this chapter, above issues are addressed by reviews, theoretical discussions and experiments.

3.3.1 Electrochemical Electrode System

A typical electrochemical cell consists of three electrodes: working, counter and reference electrodes. We are only interested in potential and excited reactions on the half-cell of the working electrode. In the three-electrode system, no current passes through the reference electrode. In a two-electrode system, the auxiliary electrode functions as both the reference electrode and the counter electrode. The potential on the auxiliary electrode is easily affected by the current passing through it, i.e. the electrode is polarized. Though the polarization effect can be reduced by increasing the size of auxiliary electrode to at least 100 times bigger than the working electrode, the drift of potential can hardly be

ignored, in terms of noise and potential control. Increasing the size of the auxiliary electrode is often not practical. In applications when high density array is required, and bulk silicon cannot be used as the auxiliary electrode, the usable chip area is limited to within dimension of millimeters. Planar electrodes are more feasible to be fabricated onto the CMOS chip surface than 3D electrodes. The chip surface is prioritized for building the high density working electrode array. In all, a three-electrode transducer provides more accurate and reliable potentiostat control to keep the protein from being accidentally denatured, as well as a less noisy current readout. Low noise is especially important to enhance the limit of detection, when the working electrode is miniaturized and the proteins do not carry out a significant current in response of excitation.

3.3.2 Geometry of Planar Microelectrode

A working electrode plays a major role in an electrode system whose performance is not only affected by its materials or modification, but also its geometric factors. A microelectrode is an electrode having its critical dimension in micrometers. As the dimension of the electrode became less than the thickness of the diffusion layer, a microelectrode or an ultra-microelectrode presents many properties that are favored in aspect of electrochemistry. A microelectrode not only has great spatial and temporal resolution, but also provides the properties of high current density, fast to achieve steady state current, low capacitance and immunity to high solution resistance. Thus, a microelectrode or UME is more suitable for electrochemical sensors on-CMOS than a regular electrode. By taking advantages of the microelectrode, the consumption of analyte can be minimized. In addition, because a microelectrode can work in a high resistance solution, a supporting electrolyte is not required, which simplifies the fluidic

delivery system and saves the precious space and weight of a portable device. On account of the low capacitance and rapid achievement of steady state current, measurement of chemical concentration can be made on a microsecond time scale [13]. Fast response of individual sensor is desired for a large sensor array. Geometric factors of other electrodes also affect the performance of the electrode system.

Planar (2-dimensional) electrode design is chosen over 3-dimensional electrode arrangement to permit the fabrication on CMOS, although 3-dimensional electrode arrangement has some advantages. Current microfabrication techniques are designed to work on a planar surface. The electrochemical lab-on-CMOS is based on an integrated circuit with its surface area in the millimeter scale, which is suitable for microelectrodes but limits the fabrication area to the small chip surface. Once built, a microelectrode can feed signals directly to the underlying CMOS circuits. CMOS and compatible microfabrication techniques, including thin film deposition, photolithography, lift-off, dry etching etc., can be employed to fabricate microelectrode system. Limiting the design to use CMOS-compatible only techniques allows the developed process to be transferred to a foundry for scaling up the production. The same microfabrication process as CMOS can construct a high density microelectrode array that improves reliability by redundancy. A microelectrode array can also accommodate several different bio-interfaces to detect multiple bio-molecules.

For a planar electrode system, the geometrical layout of the three electrodes must be optimized to performance. The working electrode and counter electrode should be placed adjacent to (1) prevent loss of energy through joule heating across the solution resistant, (2) prevent the possible change of solution micro-environment, eg. pH and (3)

reduce resistance across the solution reduces the charging time of the double layer capacitance and speeds up amperometry readout. By putting the working and the counter electrode close to each other, interference of convection along the flux between them is reduced too. Theoretically, the distance from the reference electrode to the working electrode should also be minimized to reduce the R contribution of IR loss for accurate potential control. Since the flux between the working and the counter electrode may not be uniformly distributed for a given geometry, the route from the reference electrode to the working electrode is better chosen to be at a place with less dense flux, i.e. less passing-by current, to minimize the I contribution of the IR loss. In practice, because a reference electrode is not as easy to be miniaturized, it is hard to put the reference electrode close to the working electrode. Exceptions are: the above IR loss can be experimentally determined and then electrically compensated by the potentiostat; the solution resistance is low; or enough supporting electrolyte can be added. Under these circumstances, the reference electrode could be placed away from the working electrode.

3.3.3 Electrode Materials

Materials are chosen in compatible with microfabrication, chemical environment, etc. For MSA method, the working electrode, gold is chosen because it is chemically inert. It has a wide enough electrochemical potential window for biosensor. Also, gold planar electrode is easy to be microfabricated. Furthermore, the gold-thiol bonding, a strong covalent bonding, is widely used for attaching biosensing elements. Besides, gold is also used for counter electrode material. An issue for using gold electrode is that it is not a standard foundry fabrication process. Either a costly request on change of foundry process or a post-CMOS process is required. Post-CMOS gold process can be chosen

from thin film deposition or wet chemical plating can be utilized, by weighing the pros and cons. A pro for thin film gold is its surface quality; the cons are bonding, alignment and more steps of processing compared to plating. Electroplated gold has good quality but hard to apply on aluminum and requires wirings to a power supply. Electroless plating of gold on aluminum can be done within a few steps, but the gold quality is inferior to other gilding methods.

For reference material, the Nafion-coated Ag/AgCl reference electrode is chosen over calomel reference electrode because it is biocompatible and easier to fabricate . Nafion, provided by DuPond, is a sulfonated tetrafluorethylene copolymer with both hydrophobic and hydrophilic regimes. The molecular structure of Nafion is shown in Figure 3.1. A conventional Ag/AgCl reference electrode is a surface chlorinated silver wire immersed in a 3M or 4M KCl solution to achieve constant electrochemical potential and enclosed in a cylinder with a glass frit to provide liquid junction as well as preserving Cl^- ions. As the system is miniaturized into an integrated electrochemical interface, fabrication of a planar reference electrode becomes challenging. Screenprinted silver, Nafion and other coatings over AgCl have been utilized to fabricate planar reference electrode by providing diffusion barrier, ion-selective path, and hydrolyzation-protection, at same time maintaining the inner chloride ions.

3.4 Planar Microelectrode Array

3.4.1 Design

In order to prove a post-CMOS fabrication process of a planar 3-electrode system, a prototype is designed for immobilizing enzymes.

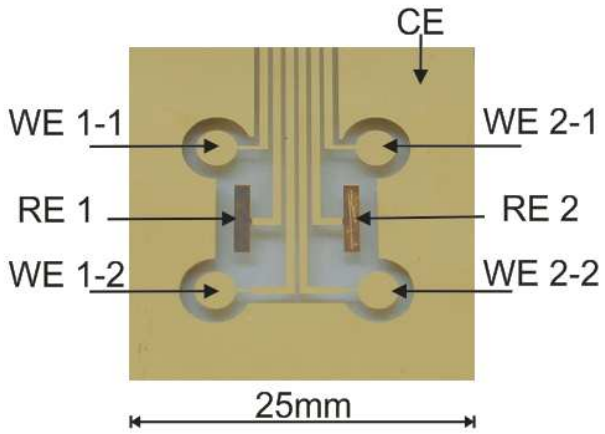

Figure 3.1: Electrochemical electrodes with 2×2 WE array and embedded Ag/AgCl RE.

The working electrodes of Figure 3.1 are 2mm in diameter, in a size that can generate enough current for a normal bench-top potentiostat to detect after enzyme immobilization. The surrounding counter electrode is sufficient larger than working electrodes. The traces leading to the working electrodes and reference electrodes are passivated with SU-8. The passivation leavings a well confined working electrode surface area of 0.0314 cm^2. The 2×2 working electrode array were grouped in two, each group shared one Ag/AgCl reference electrode.

3.4.2 Fabrication

The electrode array was fabricated on SiO_2 substrate, mimicking surface of integrated circuit for verifying process flow. As shown in Figure 3.2, the process flow for fabricating system consisted of 5 steps. The first step was a thin film deposition of 20 nm Ti/150 nm Au/200 nm Ag (Kurt J. Lesker Co., Clairton, PA) onto the SiO_2 substrate using an Edward Auto306 thermal evaporator. The second step was photolithography and

wet etching to form the electrode pattern. The positive film masks used for photolithography were generated through a 3556 dpi Scitex Dolev 450 immagesetter (Infinity Graphics, Okemos, MI). After spin coating, exposure, developing and post development baking of the photoresist, the sample was dipped in to silver etchant (NH_4OH : H_2O_2 1:1), gold etchant (I_2 : KI : H_2O 4:1:4), and titanium etchant (HF : H_2O 1 : 9) sequentially, leaving silver on all electrode sites. Step 3 was removing the unwanted silver on the working and counter electrodes with another mask, covering the reference sites for protection before dipping into silver etchant. Step 4 was to chlorinate a thin layer of Ag to AgCl by oxidizing Ag by Fe^{3+}. Researchers found out the reliability of AgCl reference electrode were proportional to the thickness of AgCl [45]. Since only 200nm Ag was deposited, Ag need to be chlorinated, while preserving a layer of Ag on Au contact without exposing AgCl to Au. 10mM $FeCl_3$ solution was used. Because AgCl has extreme low solubility product K_{sp}, which equals 1.8×10^{-10}, and the concentration of Cl^- of 10 mM $FeCl_3$ is 30 mM, AgCl can only go as high as 6×10^{-9} M in solution, from which the amount of AgCl loss can be calculated. The amount of AgCl loss was further minimized by limiting the volume of $FeCl_3$ solution being used. After chlorination, the silver chloride surface was rinsed with saturated KCl to remove absorbed Fe^{3+} and Fe^{2+}, and then dried with nitrogen. Generally, anode chlorination was an alternative iron-free method, with coulometry to determine the progress of chlorination, wherever a galvanostat is available. For our special purpose of integrated reference electrode on a circuit chip, anodic chlorination is not convenient. Gas phase chlorination of Ag is promising for the same purpose, resulting uniform and denser packed AgCl [46]. Step 5

was to cover AgCl with Nafion (Nafion 117 5% solution, DuPond) layer on the reference electrode. Nafion allows only protons to pass the membrane, thus to keep the junction conductive, while detaining the Cl^- and Ag^+ ions. With Nafion, the potential of the reference electrode was kept stable from interfering Cl^-, Br^- and S^{2-}. The Nafion was coated on the electrode and cured at 120°C for 1 h according to Moussy's method [47]. An optional polydimethylsiloxan (PDMS) mold was prepared to facilitate modification of individual working electrode as well as protecting all the other electrodes from being contaminated.

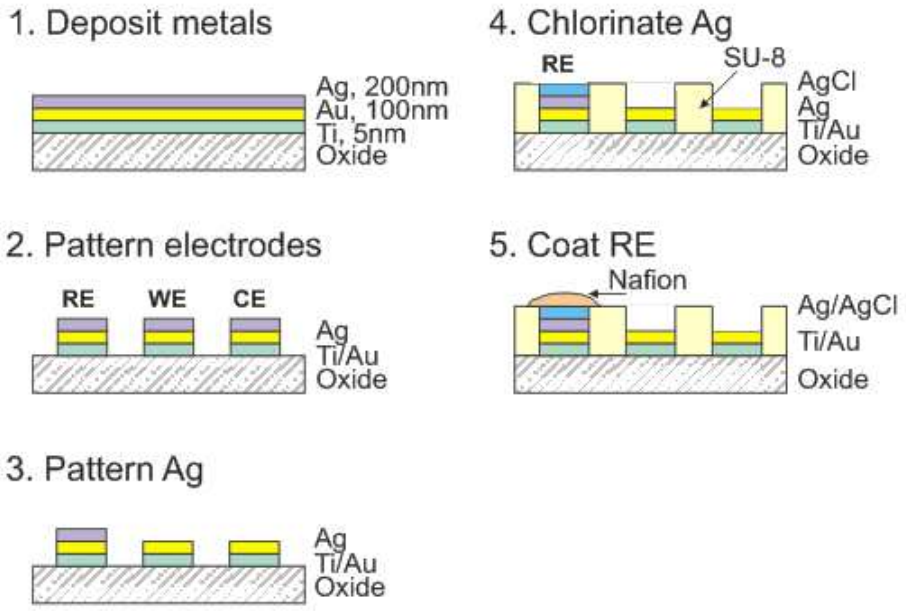

Figure 3.2: Fabrication sequence for integrated electrochemical electrode arrays with embedded Ag/AgCl reference electrodes.

3.4.3 Results and Discussion

After the electrode array was fabricated, it was characterized using cyclic voltametry. The reference electrode was first tested. The microfabricated planar Ag/AgCl

reference electrode was characterized by comparing the open potential versus a commercial Ag/AgCl reference electrode over time in 3M KCl solution, shown in Figure 3.3. The Nafion membrane was a dry film initially. When dipped in to solution, the sulfonic acid sites were hydrated for protons to tunnel through. Region A displays the membrane potential fluctuated during the progress of the hydration of the hydrophilic sulfonic acid site of the polymer. It is not preferable to use this RE in Region A. In region B, the potential is relatively stable, can be used for amperometry. The potential fluctuation was largely due to the hydration process and destruction of the Nafion membrane. After about 5h, in Region C, the Nafion membrane was not holding membrane potential, indicating the corruption of the membrane. The Nafion thin film finally failed because of hydrolysis. Since the glass frit used in commercial electrodes, there is potential difference even when equilibrium is reached. The reference electrode thus acted as it would without a Nafion layer. The reference electrode will perform like pseudo reference electrode that the potential is easily affected. It is a complex process that greatly affected the stability of reference electrode. Diffusion barrier and other membrane can be added in attempt to fortify the structure. More sophisticated coatings can improve long-term stability of microfabricated on-chip reference electrode, and applied when application requires. In next section, a coating method is developed to provide diffusion barrier and a protective layer between Ag/AgCl and Nafion. Based on the experiments, Ag/AgCl reference electrode stability needs to be improved. In Section 3.5, a Ag/AgCl/PPy(Cl^-)/Nafion quasi-reference electrodes is developed to solve the stability issue.

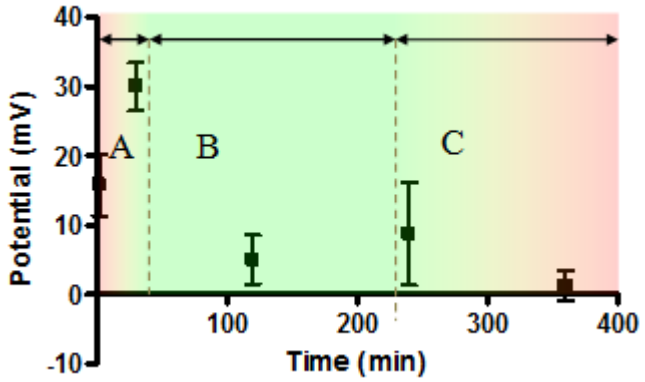

Figure 3.3: Potential difference between microfabricated planar on-chip Ag/AgCl reference electrode and commercial Ag/AgCl electrode (N=8).

Individual working electrodes are examined with cyclic voltammetry using CHI 660B potentiostat (CH Instrument, Austin, Texas) in potassium ferricynide. Figure 3.4 shows the experiment with microfabricated on-chip planar Ag/AgCl reference electrode. The peak shift due to potential difference versus commercial reference electrode can be observed as expected. In addition to being affected by the microfabricated reference electrode, the difference and variety may also cause by electrode surface conditions or convection by comparing the after-peak diffusion-limited regime approaching 0V. By using the on-chip reference electrode, the formal potential shift is 16 mV and is stable over experiments. All the working electrodes are within small variations, and can be regard as identical.

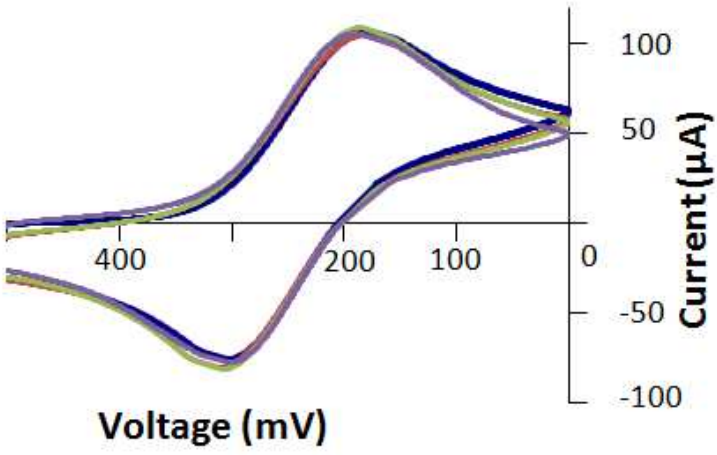

Figure 3.4: CV plots of 4 working electrodes in 10mM $K_3Fe(CN)_6$, 3M NaCl, scanning rate 100 mV/S using on-chip Ag/AgCl reference electrode.

3.5 Reference Electrode

3.5.1 Introduction

Reference electrode is an electrode which has a stable and known electrode potential. The potential represents the energy required to take a charge from one side of the electrode/electrolyte interface to the other, relates to the chemical activities of the constituents of the electrochemical reaction by the Nernst equation. By employing a redox system with constant concentrations of each participants of the redox reaction, a high stability of the electrode potential can be reached. Reference electrodes are used to determine and control an electrode of interest in an electrochemical cell. Quasi-reference or pseudo-reference electrode is so named because it does not maintain a constant potential; therefore, by definition, it is not a true reference electrode. However, its potential depends on conditions in a well-defined manner; if the conditions are known, the potential can be calculated and the electrode can be used as for reference potential.

Fundamentals of reference electrodes and review of current research can be found in [27, 48].

Common reference electrodes are standard and normal hydrogen electrode, saturated calomel electrode, copper/copper(II) sulfate electrode, silver/silver chloride electrode, palladium-hydrogen electrode, iridium/iridium oxide electrode etc. The silver/silver-chloride (Ag/AgCl) reference electrode is by far the most common type of electrode used in biosensing applications due to its simple construction and biocompatibility. According to Nernst equation, the chlorine ion acts as the chemical species in the operation of the electrode, and its activity, which is related to its concentration, has a significant impact on the electrode potential [49]. Other types of reference electrode were also developed. Yttria-stabilized zirconia membrane electrodes were developed with a variety of redox couples, e.g., Ni/NiO. Their potential depends on pH. When the pH value is known, these electrodes can be employed as a reference with notable applications at elevated temperatures. A recent advance is a metal/PPy reference electrode, which is solid-state and works in both aqueous and non-aqueous environment [50]. A solid state reference electrode is fabricated for in situ voltammetric analysis in solutions containing little or no added supporting electrolytes, coated with an electrolyte immobilized and protected with Nafion or polyurethane [51].

Microfabrication procedure of planar reference electrode includes base metal deposition and patterning, activation to create the reference material such as AgCl, and chamber interface formation. Thin film deposition, screen printing and electroplating are often used for creating a patterned metal base [45, 52-54]. Then the reference material is

applied as a form of mixture, chemically or electrochemically transformed [46, 54, 55]. The last step is coating with porous materials or gels [14, 47, 56-61].

In our integrated biosensor application, a bio-compatible solid-state quasi-reference electrode that works in buffed solution is desired. The quasi-reference electrode should be produced by microfabrication processes and can be sized to match the microelectrodes. In last section, an electrode array with Nafion coated reference electrode was fabricated. The reference electrode provides anti-interference capability.

3.5.2 Design

To miniaturize electrochemical microsystems, microfabricated Ag/AgCl reference electrodes have been investigated by Moussy *et. al* . The potential of the bare Ag/AgCl without ion-selective and diffusion barrier membranes has been observed to be affected by chloride concentration and other interferences. Meanwhile, PPy has been used for reference electrode. It can be formed on Ag/AgCl without additional patterning, and it retains Ag^{+} and Cl^{-} ions and provides ion-exchange capabilities.

The reference electrode is a crucial element in electrochemical biosensors. The size and reliability of the reference electrode are limiting factors for miniaturizing electrochemical systems. A microfabrication procedure for planar Ag/AgCl reference electrodes utilizing polymer coatings is developed. The reference electrode consists of an evaporated Ti/Au/Ag thin film with a portion of the silver chlorinated to Ag/AgCl and bi-layer polymer coatings. Electropolymerized polypyrrole seamlessly covers the AgCl to serve as a diffusion barrier and an anion exchanger. A cation exchanging Nafion coating layer compliments the ion exchange properties of the polypyrrole while blocking other

interference ions. The structure of Nafion molecule is displayed in Figure 3.5. It has both hydrophobic fluorine carbon sites and hydrophilic thiol sites.

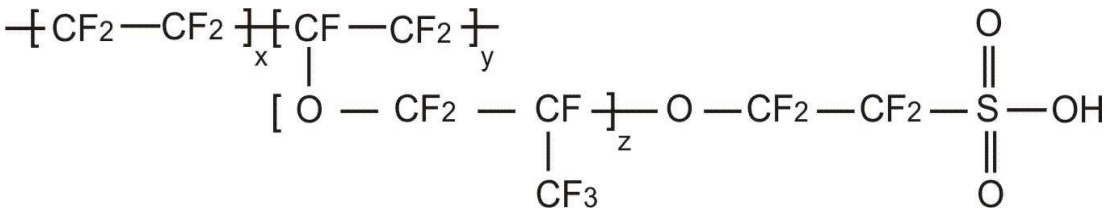

Figure 3.5: The molecular structure of Nafion.

The structure of the quasi-reference electrode is illustrated in Figure 3.6. The Ag/AgCl disk electrode is embraced by an un-closed gold ring, because Nafion was discovered having good bonding to gold because of its thiol group. PPy(Cl^-) is electropolymerized on Ag/AgCl to provide a diffusion barrier and bonding agent to Nafion.

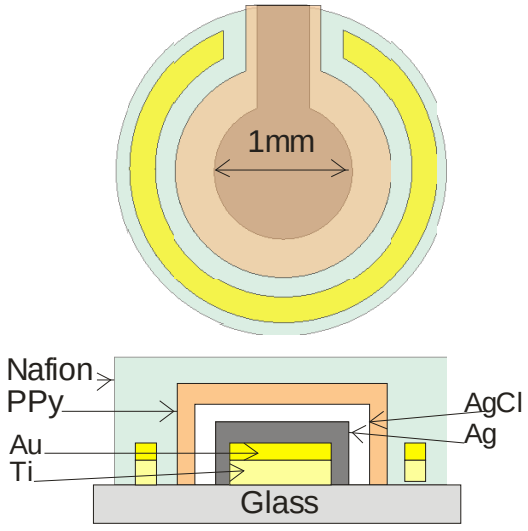

Figure 3.6: Microfabricated Ag/AgCl/PPy(Cl^-)/Nafion quasi-reference electrode structure.

3.5.3 Fabrication

Ag/AgCl/PPy(Cl^-)/Nafion quasi-reference electrodes were fabricated on a SiO_2 substrate, presented in Figure 3.3. The size was 1 mm in diameter, and can further be scaled down to microns. To achieve this, thin films of 5 nm Ti and 100nm Au were evaporated on the substrate and patterned using photolithography and wet etching to form electrode bases and traces to an edge connector. 400nm Ag was deposited over the Ti/Au adhesion layers and patterned using lift off over the reference electrode sites. The electrodes were dipped in a 10 mM ferric chloride ($FeCl_3$) solution to chlorinate ~200 nm of the silver layer to form an Ag/AgCl interface. The electrode was then dipped into 100 mM pyrrole and 1M KCl solution. By running cyclic voltammetry from 0 to 650 mV at 100 mV s^{-1} for one cycle, a layer of partially oxidized polypyrrole doped with Cl^- (PPy(Cl^-)) was formed over the AgCl. Finally, a 5% Nafion 117 solution was spun coated, cured at 120°C for 1hr, and then soaked in 1M KCl for 60 min so the hydrophilic clusters of Nafion could be hydrated to conduct protons. To characterize the electrode, the potential difference of the quasi-reference electrode, relative to a commercial Ag/AgCl reference electrode was recorded using a data acquisition card and LabView. The microfabricated Ag/AgCl/PPy(Cl^-)/Nafion quasi-reference electrode is shown in Figure 3.7:

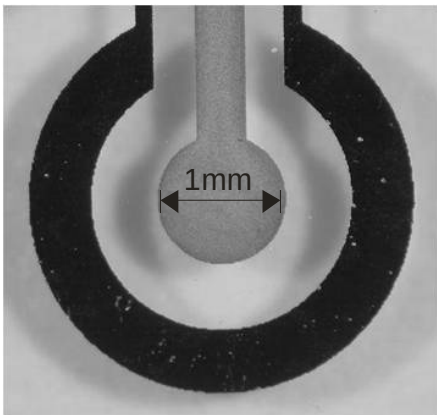

Figure 3.7: The photograph of the microfabricated Ag/AgCl/PPy(Cl^-)/Nafion quasi-reference electrode.

3.5.4 Results and Discussion

The Ag/AgCl/PPy(Cl^-)/Nafion quasi-reference electrode was tested in KCl solutions. The results show that the polymer bi-layer stabilized the potential of the Ag/AgCl system, comparing with a bare Ag/AgCl electrode in Figure 3.8. The PPy(Cl^-) provides effective chloride diffusion barrier to maintain constant Cl^- concentration at Ag/AgCl interface. The potential changes with KCl concentration because KCl affects the hydration state of the Nafion layer. Since the hydrated group passes proton, the membrane potential is affected as a result. The built-in potential of the two polymer interface with the PPy as electron donor and the Nafion as proton donor is secondly being affected by the reduced carrier concentration as a consequence of the process of dehydration due to the higher concentration of salt. The slope of potential indicates the progress of the process. The result shows that the chloride dependence is significantly reduced with the new electrode structure. Data were taken once a steady potential was reached; ramping before steady state is due to the penetration of ions across the

membrane and redox states of the PPy layer when concentration changes. Further tests in multiple interfering ions can be performed to examine its rejection to interferences.

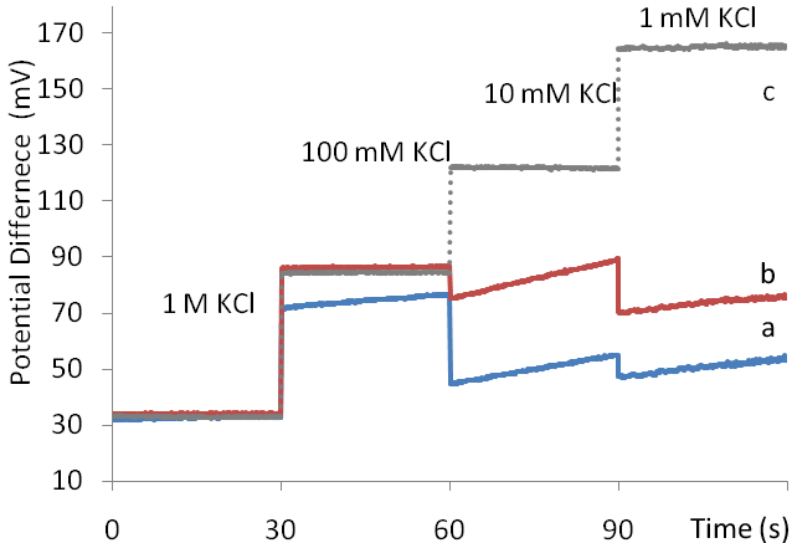

Figure 3.8: Potential difference of microfabricated Ag/AgCl/PPy(Cl-)/Nafion quasi-reference electrode vs. commercial Ag/AgCl reference electrode in various concentration of KCl. In the plot, trace a and b are the Ag/AgCl/PPy(Cl-)/Nafion quasi-reference electrode; c is a bare Ag/AgCl electrode.

The membrane potential is a function of the proton concentration in the solution. The redox state of PPy is also affected by protons crossing the Nafion layer. Figure 3.9 shows the potential difference of microfabricated Ag/AgCl/PPy(Cl^-)/Nafion quasi-reference electrodes vs. a commercial Ag/AgCl reference electrode in standard pH buffers. In the plot, trace a and b are the Ag/AgCl/PPy(Cl^-)/Nafion quasi-reference electrodes; c is a bare Ag/AgCl electrode.

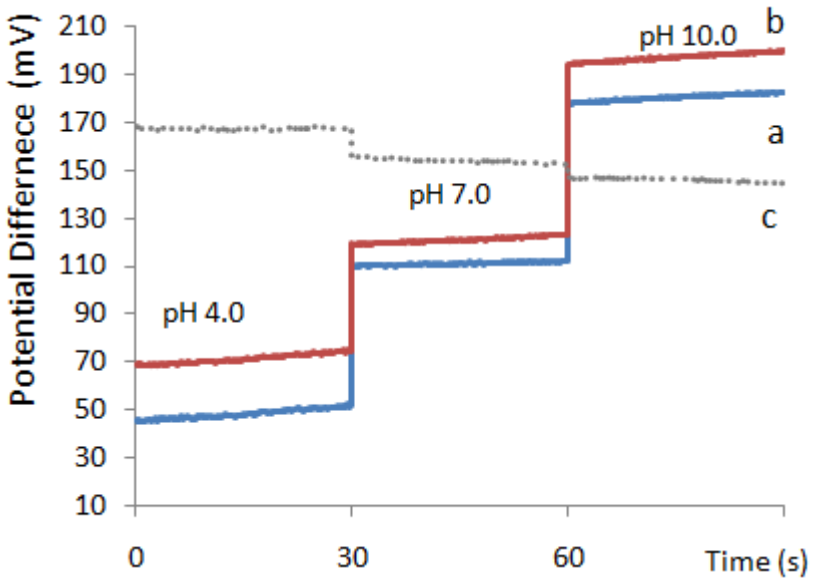

Figure 3.9: Potential difference of microfabricated Ag/AgCl/PPy(Cl^-)/Nafion quasi-reference electrode vs. commercial Ag/AgCl reference electrode in standard pH buffers. In the plot, trace a and b are the Ag/AgCl/PPy(Cl^-)/Nafion quasi-reference electrodes; c is a bare Ag/AgCl electrode.

For biosensors operating in a pH-buffered solution, the potential can be predetermined by using its potential value in standard pH buffer and Nernst equation, so the shift is tolerable. The Electrode fails after prolonged use, due in part to cracks that develop in the Nafion coating, which limits its long-term application.

3.6 Conclusion

A fabrication process for microfabricating microelectrode system on CMOS chip was developed based on the understanding of electrochemistry, within limitations of microfabrication capability. A prototype system was fabricated and tested. The working electrodes were identical and the reference electrodes were characterized. Geometry of planar electrode was discussed in order to be implemented on CMOS. To verify microfabricated electrode with enzyme immobilization, a gold electrode array was designed and fabricated. To overcome the limitation of Nafion, Ag/AgCl/PPy(Cl^-) and ph

buffered The method was identified for fabricating a reference electrode that can be miniaturized to fit on a CMOS die.

4 CMOS Bipotentiostat

4.1 Overview

A potentiostat is the instrument to control a three electrode cell and provides current readout. For enzyme biosensor array and CMOS work synergistically, redox recycling mechanism can be utilized to increase sensitivity and reduce the overall electrode area. It requires a pair of interdigitated working electrode under support of a bipotentiostat, a potentiostat capable of controlling two working electrodes respectively. In this chapter, the traditional adder potentiostat and a new architecture of a bipotentiostat are discussed in section 4.3. Redox recycling on concentric ring electrode is analyzed experimentally and mathematically in section 4.4. A CMOS bi-potentiostat is reported in section 4.5.

4.2 Background

Redox enzymes catalyze oxidation or reduction reactions with direct electron transfer, making it highly suitable for electrochemical sensors that provide continuous real-time monitoring of the target biomolecules. However, some redox enzymes have very small turnover rates, resulting in low biosensor sensitivity and low current levels when miniaturized. The redox recycling effect can be utilized to electrochemically magnify the faradic current using, for example, an interdigitated electrode array with enzyme immobilized on both working electrodes. To support redox recycling, a potentiostat must have simultaneous control of both WEs.

In the past two decades, significant research has been devoted to CMOS integrated potentiostats, which have been applied to many applications including anodic stripping voltammetry to detect heavy metal ions [21], high density electrode arrays with low current readout [62], wide potential window [63], examining DNA match [20], for reversible redox species [64], for neuron transmitters [65], with wide dynamic range [66], for detector array [54] and others. In addition to CMOS, a potentiostat was constructed using thin film transistors [49]. However, potentiostat architecture is not fully studied [67]. A CMOS potentiostat supporting redox recycling with redox-enzyme-based biosensors has not been reported.

4.3 Potentiostat Architecture

4.3.1 Electrochemical Cell and Potentiostat

In electrochemistry, a potentiostat is a piece of equipment that is used to control the potential of working electrode with respect to the reference electrode, reading out the current flow through the working electrode while the excitation wave form is applied on it. Before designing a potentiostat, the basic electrical model of the electrochemical cell is worth a discussion beyond textbook. Electrochemical cell is two or three electrode in electrolyte. It can be modeled as an impedance network tapped by connections to electrodes as symbolized by Figure 4.1(a). The key to potential control is setting a potential at the surface of working electrode, where the interested reaction takes place at this potential. In an often seen circuit equivalent model displayed in Figure 4.1(b), the surface of electrode is labeled as point A, between the working electrode impedance Z_w and uncompensated solution resistance R_u. B is the tapping point of the reference

electrode into the cell, the point of which electrochemical potential is certain. Point C is a reference point in electrical circuit. A reference electrode relates electrochemical potential to the electrical world. Also in this model, Z_C and R_Ω represent the impedance and compensated solution resistance on the counter electrode side. Notice that the total solution resistance between WE and CE is divided into R_Ω and R_u, There values depend on the tapping position of the reference electrode on the current path between counter and working electrode. A reference electrode has its impedance Z_R and solution resistance R_R, as shown Figure 4.1(c). Besides, the thermal dynamics at the solid/liquid interface established a potential, represented by E_R. In fact, there is virtually no current flow through the reference electrode. Therefore, its internal resistance, junction resistance and capacitance can be omitted. The simplified equivalent impedance network with the reference potential E_R and is shown in Figure 4.1(d).

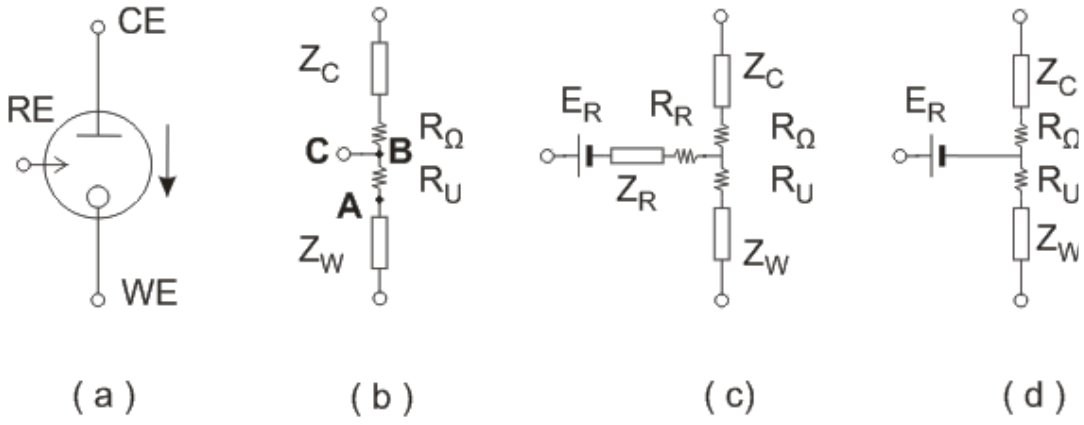

Figure 4.1: Electrochemical cell and its equivalent impedance network. (a) A electrochemical cell symbol. (b) The equivalent impedance network. (c) The impedance network with the built-in potential and impedance of RE, (d) A simplified impedance network with the built-in potential and of RE.

In an electrochemical cell the potential at the working electrode is concerned. By analyzing current responses under excitation waveforms, the reaction on the working electrode surface can be analyzed. Since the potential of reference electrode in the electrolyte is relatively stable, it is used as the reference point to control the potential of the working electrode by a potentiostat. A simple potentiostat is shown in Figure 4.2, where an op-amp is used for potential control. A stimulus E_X is inserted between RE and WE. Further, by replacing the electrochemical cell with equivalent circuit, the potential control circuit model is shown in Figure 4.3 (a). It appears more clear that the RE tapping point is biased to E_X plus E_R versus ground, and that the working electrode is grounded.

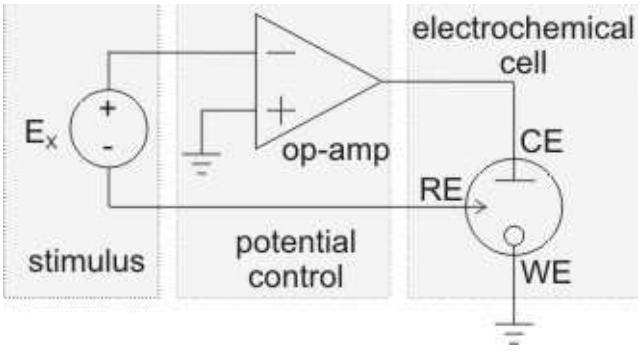

Figure 4.2: A simplified potentiostat control over an electrochemical cell.

Because of the portion of solution resistance R_u, the true potential on the working electrode is less than the desired value by an uncompensated voltage drop iR_u, called IR loss. This loss could not be eliminated, but can be reduced by minimizing R_u or be ignored if the inaccurate potential control is not significantly affecting the experimental results. Mounting the reference electrode to the vicinity of working electrode reduces R_u.

The potential control circuit applies potential through counter electrode so that the potential on the current path of current at the point of reference electrode follows the excitation signal.

An alternative scheme of potential control circuit is by inserting an excitation signal from the working electrode, as shown in Figure 4.3 (b) Scheme B. To differentiate, the scheme in Figure 4.3 (a) is referred to as scheme A. In Scheme B, the electrochemical potential of the point of tapping is controlled to approximate the same potential as reference electrode. The excitation E_X is applied from the working electrode versus ground, as shown in Figure 4.3(b).

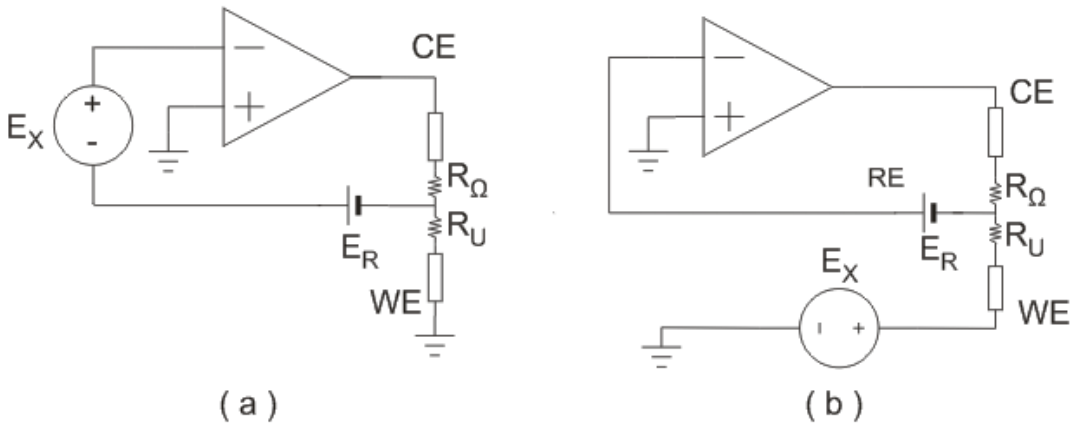

Figure 4.3: Potentiostats with the electrochemical cells being replaced by the equivalent circuit models. (a) Scheme A: The excitation signal E_X feeds through an opamp. (b) Scheme B: The exiciation signal E_X feeds through the working electrode.

To further study these two schemes, equivalent circuits of scheme A and scheme B are derived by converting the opamp negative inputs to grounds and outputs to voltage sources A_V. The two schemes of potential control circuit models are simplified for better

comparison, as shown in Figure 4.4. From Kirchhoff's voltage law, a loop voltage for the circuit in Figure 4.4 (a) is:

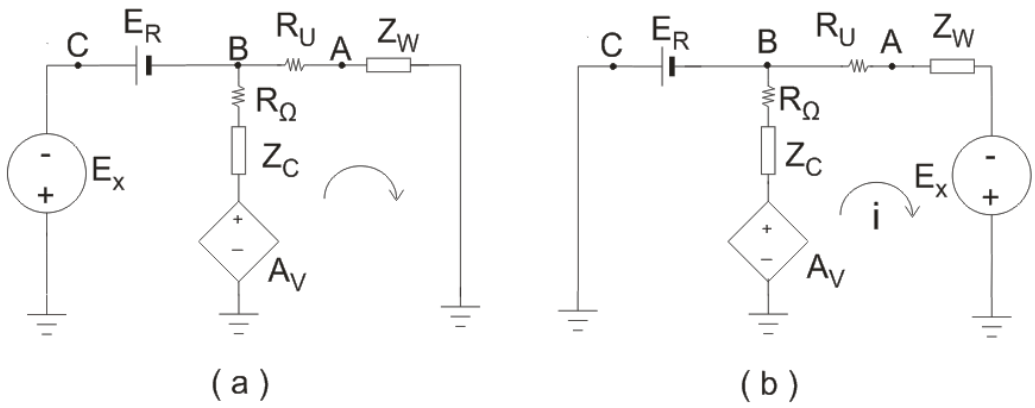

Figure 4.4: The equivalent circuit models of the two schemes of potential control and excitation signal insertion. . (a) Scheme A: The excitation signal E_x feeds through an opamp. (b) Scheme B: The excitation signal E_x feeds through the working electrode.

$$-E_X - E_R + iR_u + iZ_W = 0$$

The loop voltage for Figure 4.4 (b) is:

$$-E_R + iR_u + iZ_W - E_X = 0$$

From above circuits and equations, we can observe that the voltages across the working electrode are identical, if internal resistance of excitation is ignorable:

$$iZ_W = E_X + E_R - iR_u$$

From above equation, it is observed that the true working electrode potential versus the potential reference E_X, iZ_W- E_R equals to E_X - iR_u which is desired excitation E_X offsets by the uncompensated iR_u drop. From above analysis, the two schemes of potential control have identical equivalent working electrode potential (ignore internal resistance of excitation source E_X).

For an electrode array, it is desired that each electrode can be individually controlled by an excitation signal. To determine the suitable potentiostat architecture, the models of Scheme A and Scheme B are expanded to multiple channels, as illustrated in Figure 4.5. Scheme A requires subtracting E_x from each additional channel by additional subtractors. The control scheme B in is more hardware efficient for applying excitation signals on the multiple electrodes. As of electrode geometry for both control schemes, it is equally important to position the working electrode as close as possible to reduce R_u whenever possible.

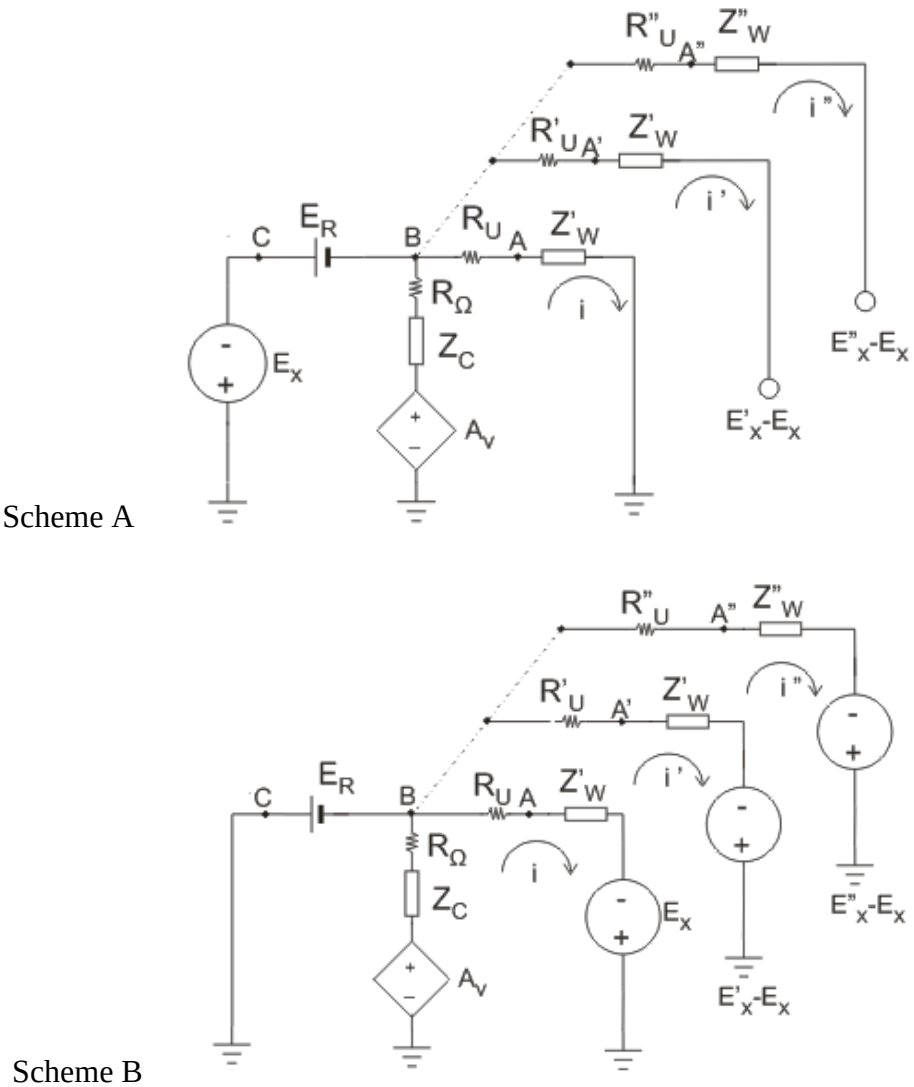

Figure 4.5: The equivalent circuit model of expanded Scheme A (top) and Scheme B (bottom) to multiple channels;

4.3.2 Bipotentiostat Architecture

In some electrochemical experiments, two working electrodes are required to individually controlled and work simultaneously. The electrochemical instrument is called bipotentiostat. In Section 4.3.1, potentiostat models were expanded to support array. Those models can be simplified to support two channels. The potentiostat of Scheme A in Figure 4.5 is called “adder potentiostat”, because the excitation signal is

added to the reference potential at the inputs of an analog adder. A circuit to implement the scheme is comprised of buffers and current to voltage converter.

In the adder potentiostat, the potential at the reference electrode tip approximates the true potential on the working electrode in vicinity, equals to the excitation signal for this first working electrode. To adapt an adder potentiostat to simultaneously control a second working electrode by this approach, the excitation potential is subtracted from the excitation signal of the second working electrode through an analog subtractor, as shown in Figure 4.6. The resulting signal is the difference of the two signals, used to bias the second working electrode. At the interface of 2^{nd} electrode, the potential difference versus the 1^{st} excitation signal recovers the 2^{nd} excitation signal.

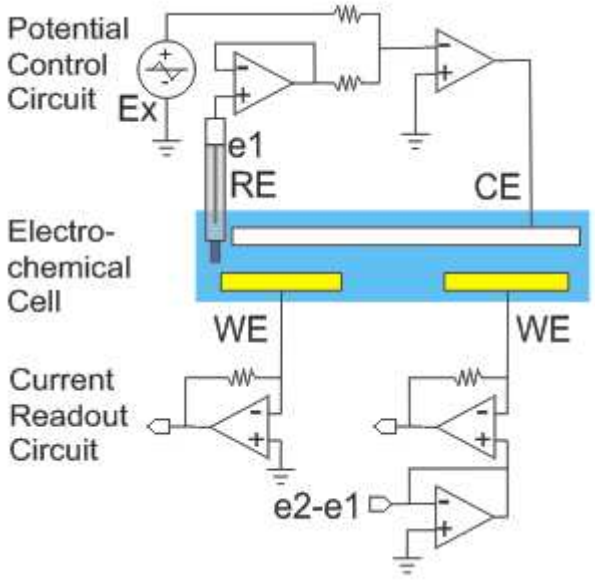

Figure 4.6: A bi-potentiostat based on traditional adder potentiostat architecture.

The above adder potentiostat approach is complicated in potential control because it employs the potential of the first working electrode. Moreover, the error introduced by the uncompensated potential loss as shown in the equation below is propagated to the second working electrode.

$$E_X = iZ_W - E_R + iR_u$$

An alternative approach is as suggested by the above analysis in section 4.1, removing the excitation signal from the adder and biasing the working electrode with it. In this approach, the reference potential is disassociated with excitation signal, so each working electrode is biased with the original excitation signal without additional arithmetic processing, as illustrated in Figure 4.7.

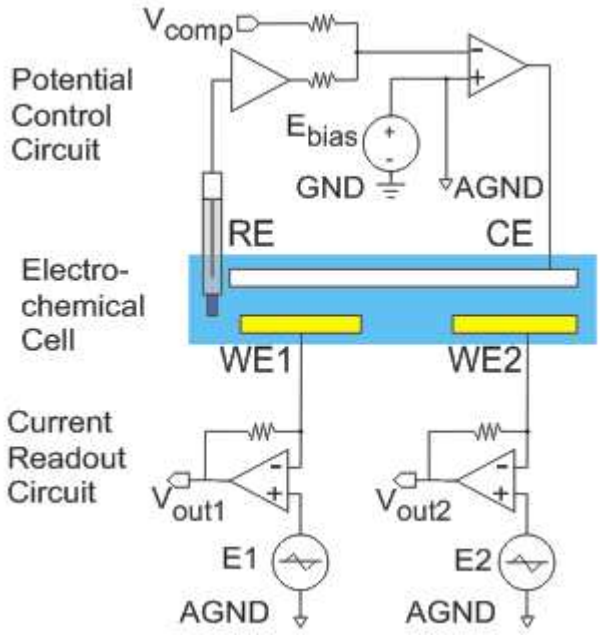

Figure 4.7: (a) A bipotentiostat by expanding Scheme A, the traditional adder-potentiostat architecture. (b) A bi-potentiostat for electrode array based on Scheme B with two parallel channels.

As a result, Scheme B saved two opamps for performing inversion of e2 and subtraction of e1 out of e2, compared to Scheme A potentiostat circuit illustrated in Figure 15.46 in Bard's book [26]. Because of these benefits, the Scheme B architecture is adopted. The impact of saving two opamps on CMOS layout is discussed in Section 4.5.

4.4 Redox Recycling on Concentric Ring Electrode

4.4.1 Background

The current of enzyme biosensor is a function of enzyme activity, electrode geometry and substrate concentration. For on-chip enzyme modified electrode, the chip surface area is limited and the enzyme activity is fixed. Increasing the sensitivity of the sensor can reduce the sensor footprints to allow more sensors on the chip surface.

4.4.1.1 Redox Recycling

We assume the reversible reactions below take place on a pair of electrodes at reduction potential and oxidation potential respectively:

$$R - ne \leftrightarrow O$$

$$O + ne \leftrightarrow R$$

where R and O represent the reduction and oxidation state, n is the number of electrons involve in the reaction, and e is an electron.

In traditional electrochemical system, the species including the concerned analytes migrate toward the working electrode and leave the electrode surface after being transformed. The reverse transformation will not happen until a favoring potential being applied. The current is limited by mass transfer including diffusion and migration when

the species are transformed quicker than replenished. The migration is proportional to the electric field strength. According to Fick's law of diffusion, the current density is proportional to the bulk concentration of the species being transformed. For a given size of electrode, the detection limit is thus limited.

$$J = -D\frac{\partial C}{\partial x}$$

To improve the limit of detection on an electrode of determined size, an additional working electrode can be situated close by, preferably within the distance of the diffusion layer l, determined by equation below:

$$l = \sqrt{2Dt}$$

where D is diffusion coefficient, t is the time span of experiment. The limit of detection can be improved in several aspects by this additional working electrode. By setting it to a potential of the reverse reaction, the transformed species consumed at one electrode are reproduced at the other, locally increasing the concentration of the reacting species, thus to increase the concentration gradient for diffusion and current density in consequences. In addition it increases the electric field by a larger potential difference and a shorter distance, promoting the migration of charged species thus increases the background current as well. Since the species being reduced or oxidized at one electrode and oxidized or reduced on the other without diffusing into the bulk solution, it reduces the invasion of the environment being tested. This is known as "redox recycling".

To realize redox recycling, the two electrodes of an interdigitated band array are often set to reduction potential and oxidation potential respectively. It also requires a bipotentiostat to control the potential on each electrode independently. The geometry of the interdigitated array electrode (IDA) and bipotentiostat are discussed further in the next sections.

4.4.1.2 Concentric Ring Electrode

From the discussion in previous section, an IDA has some advantages over a traditional disk electrode. From the analysis, the steady state current of an IDA, unlike disk electrode, is a function of time, though ignorable when the length to width ratio is sufficiently large [26]. The disk electrode is stable at steady state, but the interior of the disk supports very little electrochemistry so can be eliminated. The resulting ring electrode resembles the behavior of a disk electrode and is more area-efficient. A carbon film-based interdigitated ring array electrodes was designed as detectors in thin-layer radial flow cells [68]. A e-beam lithography microfabricated gold ring electrode array was constructed for redox chemicals [64]. Not only in electrochemistry, were ring electrodes also applied for detecting surface electromyographic signals with high spatial selectivity [69].

The concentric ring structure combines disk and IDA, and can benefit from both of the advantages and avoid the disadvantages. As an example shown in Figure 4.8 shows a 90 µm concentric ring electrode fabricated on a 0.5µm AMI C5N CMOS process through MOSIS.

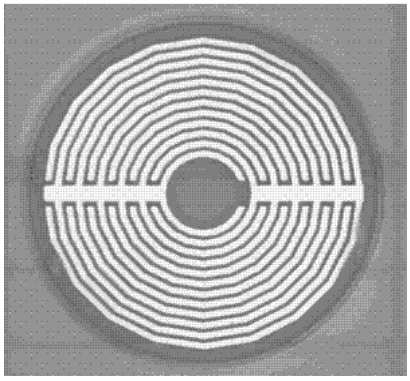

Figure 4.8: An exampleconcentric ring electrode fabricated on a bipotentiostat chip by CMOS 0.5 μm technology. The diameter of the outer ring is 90 μm.

A mathematical model was developed based on diffusion equation, and its boundary conditions were defined in Appendix. This model can be used for finite element analysis using software tools such as COMSOL MultiPhysiscs to estimate the diffusion current at redox recycling to evaluate the electrode geometry factors.

4.4.2 Fabrication of Concentric Ring Electrode

To investigate the redox behaviors on a concentric ring electrode, a concentric rings-disk electrode was fabricated. It comprised of two neighboring ring working electrodes, an outer ring counter electrode and an inner disk reference electrode. The disk electrode in the center is in a diameter of 2.54 mm. The disk electrode is surrounded by three concentric ring electrodes each has an opening at the same direction for wiring. The first, the second, and the third rings are 0.7 mm, 0.5 mm, and 0.75 mm width, respectively, noted as WE1, WE2 and CE respectively. The gap between the first and the second ring electrodes and the second and the third electrodes are 50 μm and 250 μm, respectively, shown in Figure 4.9.

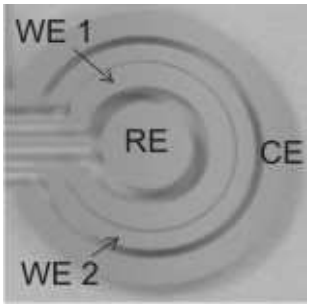

Figure 4.9: A concentric ring electrode fabricated on glass substrate, including two neighboring working electrodes, WE1 and WE2, a surrounding ring counter electrode and CE a disk reference electrode RE.

The electrode in Figure 4.10 was prepared by physical vapor deposition of 5nm Ti followed by 100nm Au on glass slides. Then photolithography and wet etching were applied.

4.4.3 Results and Discussion

To explore the redox recycling capability of the electrode in Figure 4.10 was coated with ionic liquid $BMIBF_4$ to study the redox behaviors of nitro aromatic compounds. $BMIBF_4$ is able to absorb nitro compounds vapor such as ethylnitrobenzene (ENB) in atmosphere. The electrochemical measurements were done with an EG&G 273 potentiostat. The scan rate of cyclic voltammetry was 100 mV/s. Differential pulse voltammetry (DPV) was done with a pulse height of 25 mV, a scan rate of 20 mV/s, and a pulse width of 50 ms.

The experiment was conducted in air and in 1 mM ENB in $BMIBF_4$. The results of CV showed the two reduction processes of the ENB shown in Figure 4.10. Typically, a reversible reduction and a consequent irreversible reduction were observed. The first

reduction peak at -1.7 V (vs. Au) corresponds to the reduction of the nitro ($-NO_2$) group to a nitro anion radical ($-NO_2^{-\cdot}$). In most electrolyte solutions this reduction is electrochemically and chemically reversible. The second reduction of ENB at -2 V (vs. Au), mostly irreversible, is related to the protons in the electrolyte solutions. In this step, the nitro radical anion is further reduced to nitro dianion and eventually hydroxylamine. The oxygen peak at -1.25 V (vs. Au) in air can be observed in ENB saturated air, and can be used as a reference.

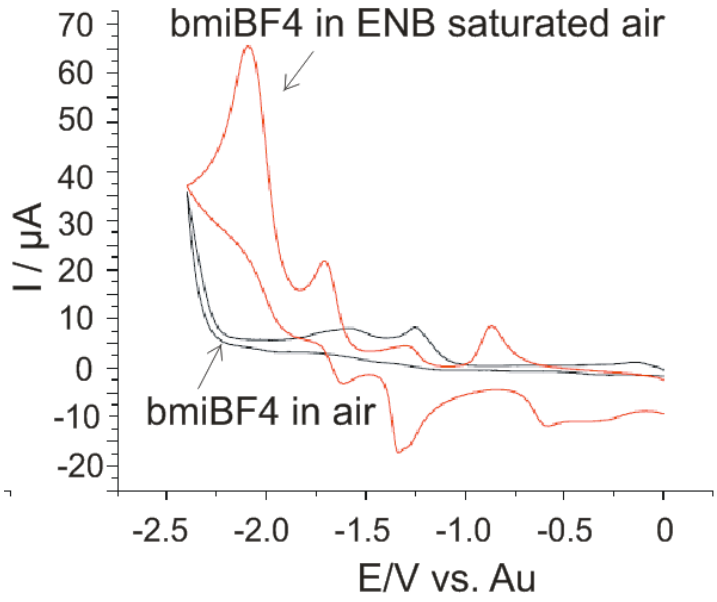

Figure 4.10: CVs of bmiBF4 exposed in air and in ENB saturated air.

DPV was conducted to help identify the redox recycling. In the experiment, one working electrode was fixed beyond the oxidation potential of nitro anion radical at -1.6 V (vs. Au). Te differential pulse was applied on the other working electrode and the current was plotted. A magnified reduction current can be reserved, which is due to the

regenerated nitro group. On the contrary, the other peak was diminished because the oxidation reaction was irreversible. It's unable to be replenished once consumed, even though the potential on the other working electrode was set to a potential beyond its oxidation point.

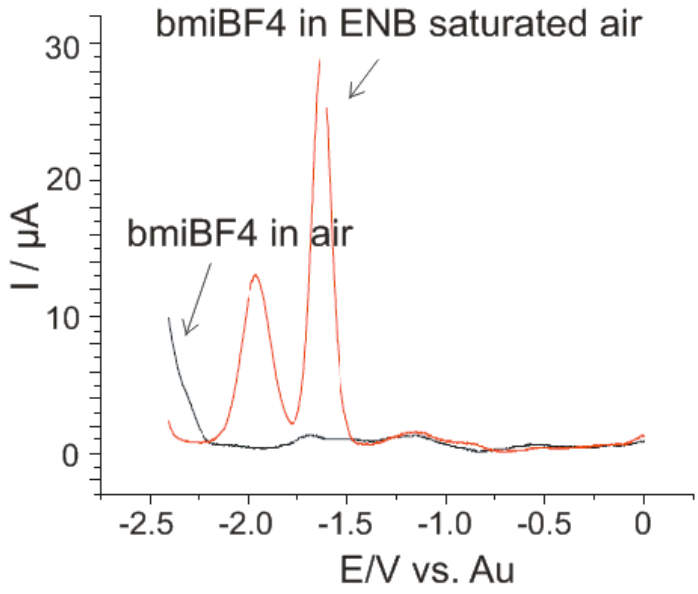

Figure 4.11: DPV plots of bmiBF4 exposed in air and in ENB saturated air.

The above results experimentally proved the current magnification effect of a redox reversible species on a microfabricated concentric ring electrode. From these result, we can predict that it is promising that a similar current magnification effect will work on an enzyme-modified concentric ring electrode.

4.5 Result and Discussion

A CMOS bipotentiostats were fabricated using AMI 0.5µm process through MOSIS [14]. The feedback resistors were replaced by switching capacitors for better

matching in the trade-off of control complexity. The bipotentiostat is constructed by using the op-amps from the earlier adder potentiostat. In this CMOS bipotentiostat, the potential control pin V_{comp} is tied to ground. The two readout circuits are in parallel. The two excitation signals bias the two working electrodes. The functional structure of the circuit is as shown in Figure 4.8. The chip also carries an on-chip three by three electrode array formed on top of CMOS metal 3, including a set of concentric ring working electrodes locate in chip center.

Figure 4.12 below shows the layout of the CMOS bipotentiostat with concentric ring electrode on the chip. The chip size is 1.56×1.69mm. Each readout channel occupies 600µm×280µm, or 0.168 mm^2. The two opamps in the potential control block used two identical class A-B opamps, 390µm×173µm each, or 0.067 mm^2. If an adder potentiostats were to adopt those opams in their readout arithmetic circuits of additional channels, each channel uses two additional opamps, the extra area would be 0.134 mm^2. Based on above assumption, each additional channel of a potentiostat using the new architecture saves 44.37% area.

The offsets were tested and adjusted through the V_{comp} input. By connecting WE1 or WE2 to a Keithley 2400 source meter, the current to voltage (-V) converter readout channel was characterized for subsequent measurements. Figure 4.13 shows the I-V converter calibration curves ranging from 10 µA to 10 nA, adjusted by changing the clock frequency.

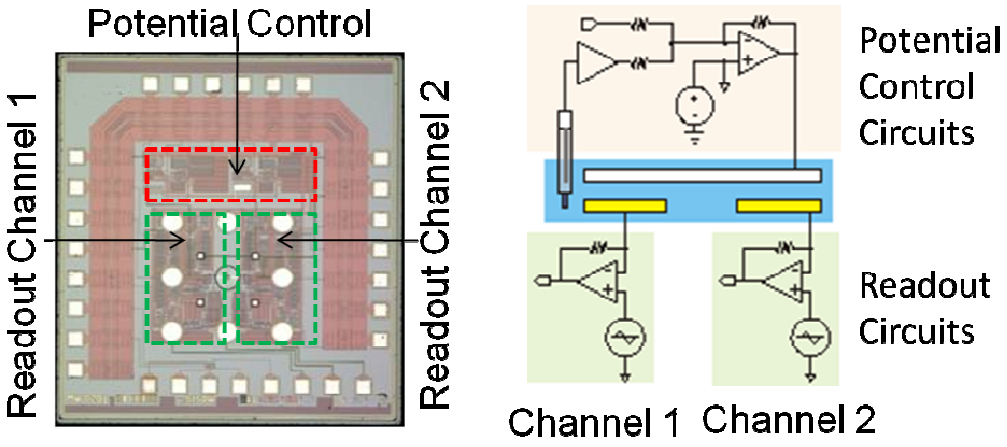

Figure 4.12: A CMOS bipotentiostat with concentric ring electrode and the circuit architecture. The chip size is 1.56×1.69mm.

The final test steps include circuit test, sensor test and final system test. The integrated potentiostat works in either single channel mode or dual-channel bipotentiostat mode. The test of the potentiostat follows the published method as the previous version of potentiostat. Once configured in bipotentiostat mode, it is to adapt concentric ring electrode to readout the current on both generator and regenerator electrode. The packed integrated potentiostat die is to be tested before enzyme is being immobilized on.

The example fructose biosensor was assembled on a 5 mm by 5 mm IDA fabricated on oxidized silicon using photolithography, deposition of Ti/Au and lift-off. The IDA had 5 μm wide fingers and 5μm gaps. The MDH enzyme was immobilized on the IDAs following published procedures [10]. It was then fixed in glutaric acid for 20 minutes. The functionality of the MDH modified IDA was tested using a CHI 760 commercial bipotentiostat in the presence of 200 mM D-fructose in pH 6.0 phosphate buffer solution. A platinum counter electrode and an Ag/AgCl reference electrode were used for subsequent experiments.

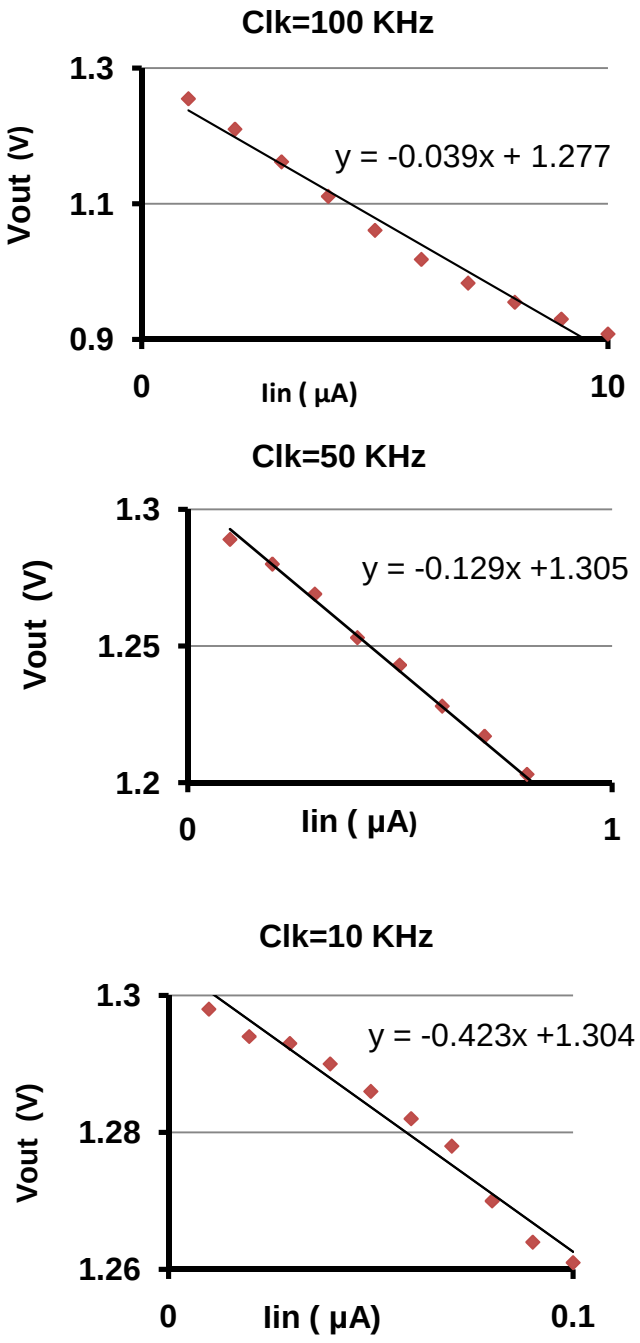

Figure 4.13: Readout opamp I-V conversion output at 100 KHz, 50 KHz and 10 kHz clock frequencies.

A cyclic voltammetry experiment of redox recycling was conducted by sweeping the potential on WE1 while WE2 was set to 0.2V. Figure 4.14 (a) shows the D-fructose reduction peak at 0.03V and the D-mannitol oxidation peak at about 0.2V vs. Ag/AgCl. This data established the potential range for subsequent chronoamperometry experiments. As expected, the cyclic voltammogram shows a reduction peak current under redox recycling (3.3nA) that is 27% higher than without redox recycling (2.6nA), demonstrating the enhanced sensitivity of redox recycling.

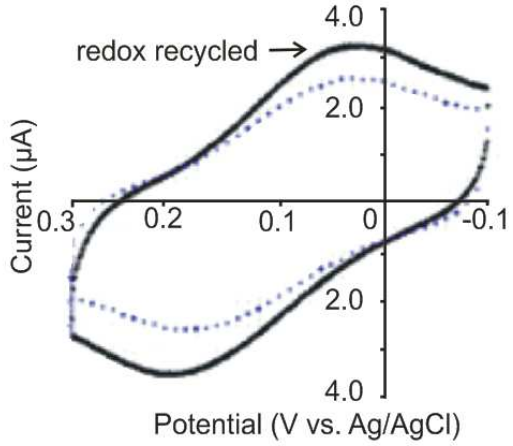

(a)

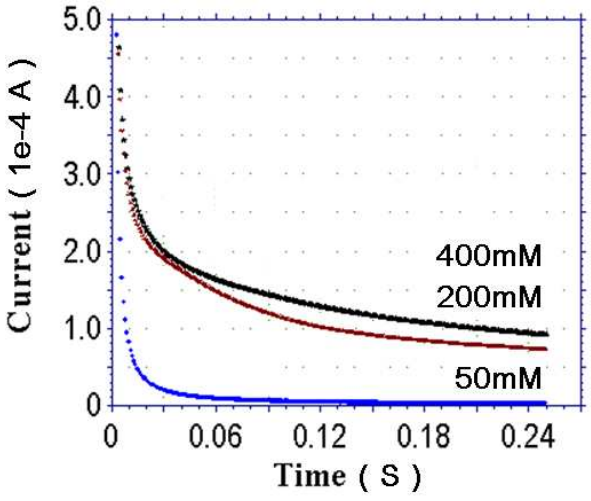

(b)

Figure 4.14: D-Fructose sensor response on MDH modified IDA. (a) Cyclic voltammetry of 200 mM D-furctose with (solid) and without (dotted) redox recycling (top). (b) Chronoamperometery of 400 mM, 200 mM and 50 mM D-fructose with redox recycling (bottom).

In a chronoamperometry experiment, in order to measure the fructose concerntration, the commercial bipotentiostat was configured by setting to perform a potential step from E1 at -0.1V on WE1 to E2 at 0.2V on WE2 versus an Ag/AgCl reference electrode. The steady-state currents were recorded at 250ms after applying the potential steps. Then the CMOS bipotentiostat was connected to the fructose sensor to perform above chronoamperometry in 100mM, 200mM and 300mM fructose solutions. The output voltage was converted to concentration using the I-V calibration curves. For comparison, chronoamperomtetry experiments were repeated using a commercial bipotentiostat in 400mM, 200mM and 50mM fructose solution. The fructose concentration measured by both CMOS bipotentiostat and commercial bipotentiostat are plotted in Figure 4.15, demonstrating that our CMOS bipotentiostat shows good agreement with standard commercial instrumentation. This research was published in

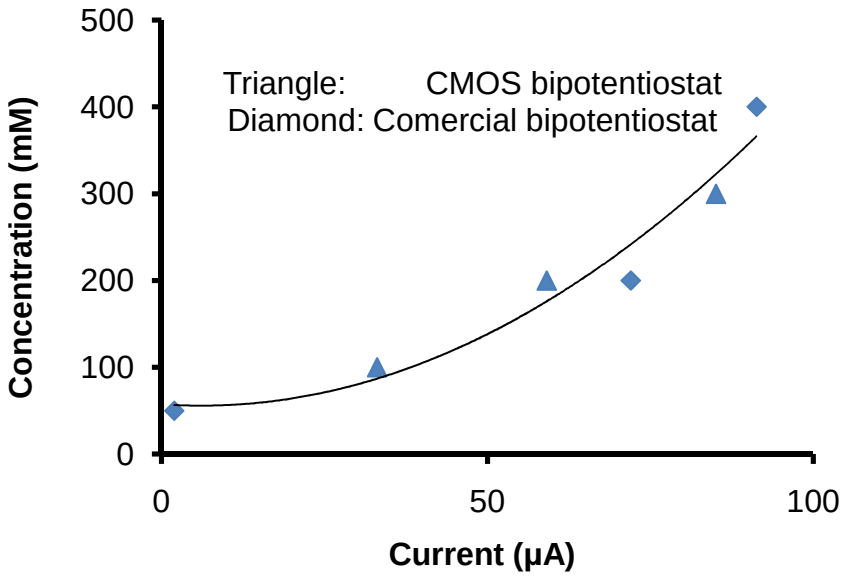

Figure 4.15: Fructose concentration vs. current measured by a commercial potentiostat and the CMOS bipotentiostat. Diamond marked data is from CHI 760 bipotentiostat. Triangle marked data are from the CMOS bipotentiostat.

[14].

4.6 Conclusion

A new bipotentiostat architecture was constructed to replace bipotentiostat based on traditional adder potentiostat. A CMOS bipotentiostat was structured to support redox-enzyme-based biosensors, providing simultaneous potential control over two WEs, sufficient potential window and current readout range, flexibility for offset adjustment. The new architecture saves 44.37% area for each additional channel implemented using AMI $0.5\mu m$ CMOS process and previously published opamp. A redox-enzyme-based biosensor was shown to work seamlessly with the CMOS bipotentiostat in applying chronoamperometry to determine biomolecule concentration. A fructose sensor was created by molecular self-assembled MDH on a microfabricated gold IDA. Interrogated in the redox recycling mode, the sensor exhibited an enhanced sensitivity of 27%. Chronoamperometry experiments using the CMOS bipotentiostat showed good consistency in accordance with a commercial bipotentiostat. Success with the fructose sensor suggests that, by exchanging the redox enzyme, the CMOS bipotentiostat can be used to enhance sensitivity of other redox-enzyme-based biosensors for detecting glucose, alcohol and other important biomolecules.

5 Lab-on-CMOS System Integration

5.1 Overview

The advance of IC technology allows integrating an electrochemical instrument on a single chip, such as potentiostat and impedance spectroscopy circuits. Using the microfabrication technique employed by IC industry, microelectrodes can be directly formed at the time of ICs fabrication by foundry, or after foundry by post-CMOS process, allowing on-chip chemical sensing. Biosensing capability can be added to the electrode by immobilizing biosensing materials. The challenges of integrating biosensors on CMOS die exist on their compatibilities during processes and tests. The sensors must be in contact with the solution, but the circuits must be protected from liquid [63]. CMOS chip should avoid being contaminated of alkali, copper or other ions; otherwise, those ions will diffuse into silicon and cause drifting of threshold [70]. Processes in high temperature and would cause CMOS material degeneration, eg., aluminum alloy. High electric field will cause migration of electrons, accumulation and breakdown [71]. Passivation materials should be biocompatible and able to survive harsh chemical environment. All materials should be compatible with microfabrication.

Electrochemical biosensor sensors, corresponding readout circuits, and sample handling microfluidic devices have been realized with CMOS and CMOS-compatible processes. However, a distinct lack of integration of these components remains as a major obstacle toward miniaturization of the entire system. A few researchers have been attempting to integrating biosensors directly on CMOS dies. The few known CMOS-microfluidic integration approaches have been built upon wirebonded die in industry

standard packages. Hindered by bonding wires, incorporating complex microfluidic structures has not been achieved. CMOS die level integration provides opportunities to improve packing density [18]. The reliability of microfabricated planar interconnects on pre-fabricated CMOS has been demonstrated [23]. So far, CMOS die level packaging with microfluidic using microfabricated interconnects has not been reported.

This chapter describes a die level CMOS-microfluidic integration approach using microfabricated interconnects routing signals from a CMOS die padframe to edge of a carrier chip to create an extended planarized surface for complex microfluidic structures. Key features of this new "lab-on-CMOS" process include complex microfluidic structures and batch-fabrication capabilities. This thesis work reports the lab-on-CMOS integration scheme and its application on enzyme-based biosensors. Major processes include electroless plating, microfabricated planar wiring, silicon chip carrier micro-machining, surface leveling, metallization and planarization. The CMOS potentiostat reported in Chapter 4 is prepared and packed into a silicon carrier by those processes and then integrated with a PDMS microfluidic mixer.

5.2 Packaging a CMOS Die for Microfluidics

Biosensor formation and test in ion containing liquid environment is detrimental for CMOS. Ion solution is conductive, can cause CMOS short circuits if exposed. Some ions, such as alkali and copper diffuse quickly in silicon will cause transistor threshold drifting, and unrecoverable circuit malfunction. A general rule is that only the electrodes should be exposed to the solution. The rest area of a CMOS die must be properly passivated to block the circuit from contacting with liquid.

Another challenge is incorporating high density microfluidic structures with CMOS. CMOS package should provide real estate that accommodates complex microfluidic structures with micro channels running across the chip. A planar surface is desired for leakage-free bonding and continuous fluid flow. Microfluidic channel crossing the chip edge over to chip should be even and continuous to eliminate turbulent flow. The packaged CMOS should survive harsh chemical environment during enzyme-based biosensor formation, and the packaging process should not denature the enzyme.

CMOS-microfluidics integration works were done on top of a factory packed chip. In this approach, a CMOS die is seated on bottom of the open cavity of an industrial standard dual inline package (DIP) or quad flat package (QFP), with the CMOS pads wirebonded to contacts around the perimeter of the cavity. The exposed metal bonding wires, the bonding ball and the pads should be insulated. Obviously, the bonding wires are obstacles for incorporating microfluidic structures. The bonding of microfluidic structure to the chip should be enduring and leakage free. Researchers have been unsuccessful in dealing with above issues. Other industrial standard IC packaging technologies, such as chip size package (CSP) and ball grid array (BGA), use solder bumps instead of bonding wires and have higher packing density. However, the solder bumps elevate the chip surface level, and are still obstacles for microfluidic channels. CMOS-microfluidic integration on those types of package have not been reported so far.

This research uses microfabricated planar interconnects and passivation to provide planar surface for microfluidics for enzyme-based biosensor integration. Microfluidic structures can be added on after enzyme immobilization. Key processes

such as leveling, planarization, low temperature PECVD oxide for permanent PDMS bonding were used to resolve the challenges.

5.3 Lab-on-CMOS Integration Procedure

An even and continuous flat surface is the key to successful lab-on-CMOS integration introduced in Section 1.1. High quality photolithography is fundamental for microfabrication, requires a flat surface to dispense, expose and develop photoresist evenly. A flat surface is essential to planar interconnection and microfluidic sealing and continuity. A carrier is placed on a silicon wafer which serves as a flat bed. A CMOS die is flipped, facing down to the flat bed, fitted into the cavity and fixed. The chip and carrier assembly is released from the flat bed.

The lab-on-CMOS integration process flow is illustrated in Figure 5.1. After the chip is prepared by gold plating, a silicon carrier is prepared using DRIE to create a cavity in size of the chip, with some tolerances, as shown in Step 1. The second step is to mount the chip and carrier on a wax covered glass wafer with their face down, followed by a fixing step, Step 3, to fill the trench between chip and carrier with filling materials such as epoxy and to cap the opening to improve mechanical strength. Then the CMOS chip and silicon carrier assembly is released from the glass wafer, cleaned and coated with a thin layer of polyimide around the gap between the CMOS chip and carrier, shown in Step 4. In Step 5 and Step 6, the assembly is metalized with thin film gold and passivated with thick polyimide and oxide to further planarize the surface. Step 7 opens the polyimide above the electrodes, exposing the electrodes to fluid. Then the electrodes

are ready to be modified by enzyme. In Step 8, a PDMS optional microfluidic structure can be added onto the assembly.

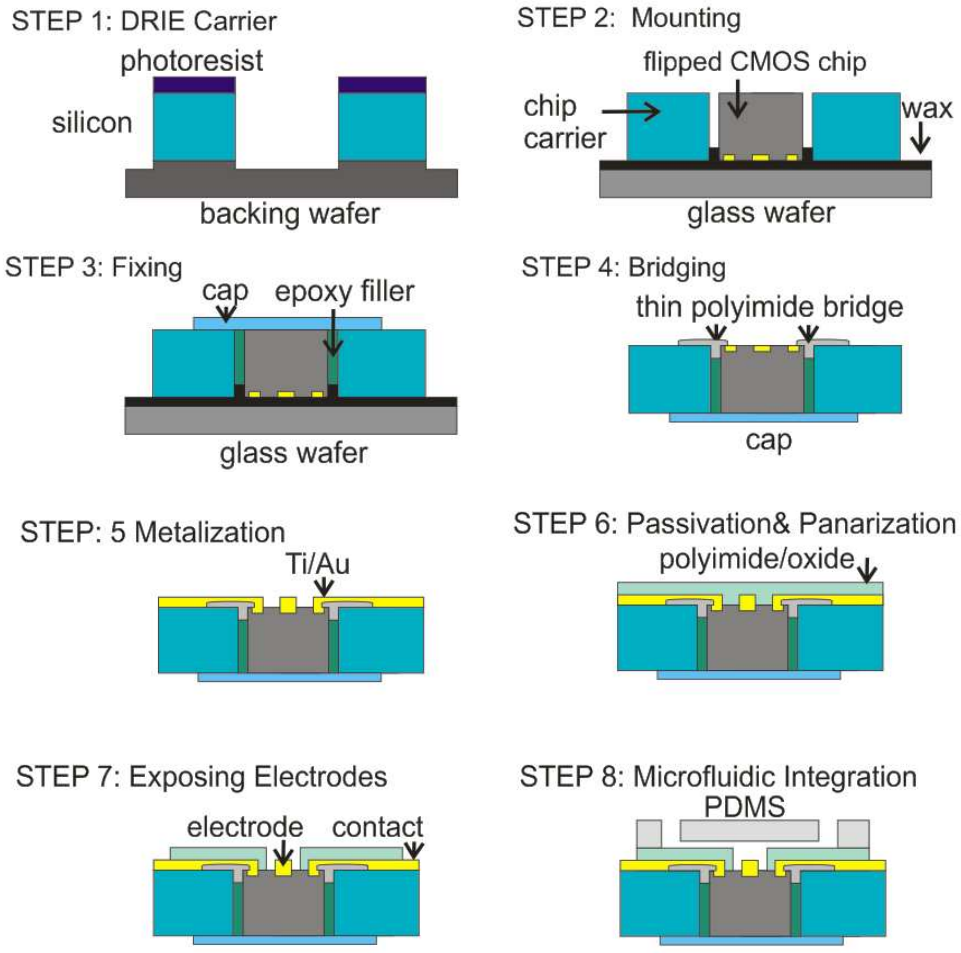

Figure 5.1: Lab-on-CMOS integration process flow.

5.3.1 CMOS Die Preparation

Aluminum pads and electrodes on the CMOS die were plated with gold over to avoid corrosion due to hydroxide in common photoresist developer. Electroless gold plating over CMOS aluminum has been proven to be successful [23, 72, 73]. In this process, the CMOS die was cleaned to remove organic contaminants, then was etched slightly with aluminum etchant to remove aluminum oxide and expose fresh aluminum.

An intermediate zincation step replaced a thin layer of aluminum with zinc to permit subsequent deposition of a nickel film. After cleaning the nickel in dilute hydrochloride acid (10%) briefly, gold plating was performed by dipping the CMOS chip into immersion gold solution. Zinc, nickel and gold plating solutions were acquired from Transene Company (Danvers, MA). To examine the plated gold, a pad was cross-sectioned using focus ion beam. As shown in Figure 5.2, about 2µm plated metals fills the contact opening without noticeable metallization on the overglass surrounding the contact. To verify if the metals would survive chemicals used in photolithography, the chip was then soaked in 5% sodium hydroxide for 30 minutes. No sign of attack on the metals was observed under a microscope, indicating the chip pads are safe for photolithography using hydroxide based developer.

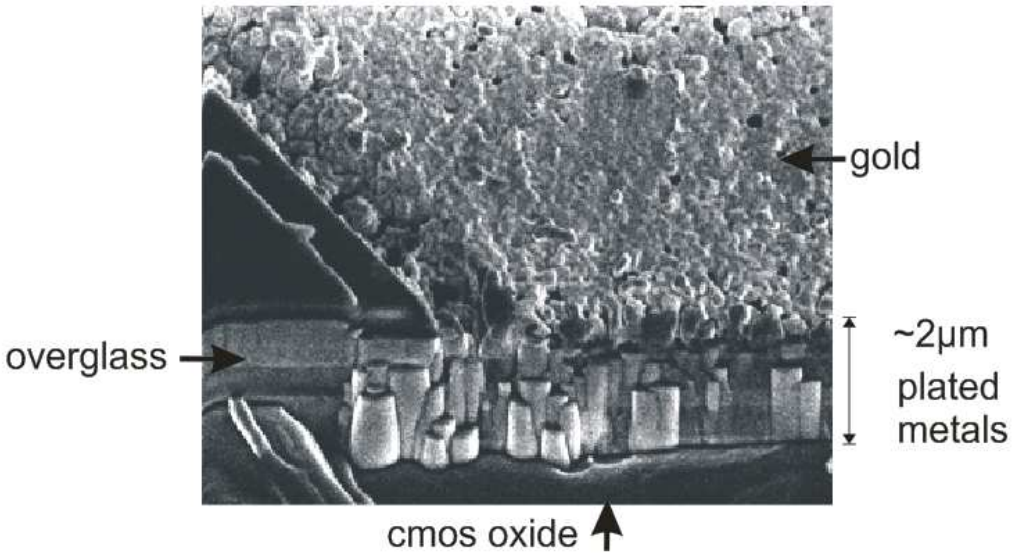

Figure 5.2: A cross-section view of a CMOS pad after electroless plating of zinc, nickel and gold.

5.3.2 Silicon Carrier Micromachining

A silicon chip carrier was used to host the CMOS chip and broad the surface to match a microfluidic device. A silicon chip carrier s prepared by etching a cavity through a silicon piece that would hold the CMOS chip. To form the cavity, potassium hydroxide (KOH) wet etching and dry etching were evaluated. KOH wet etching through a (100) silicon wafer creates sidewall slopes. Mask design for wet etching should compensate undercuts and sidewall slopes. Double side polished wafer should be used to allow photolithography on both side. Dimension control over the opening is challenging partly due to undercuts and the inconsistent etch rate across the cavity caused by bubble-trapping especially when etching goes deep. The resulting wide opening on one side of the silicon carrier facilitates chip placement and provides self-adjusting by gravity, but the chip tends to lean and rotate in the cavity. Compared to KOH wet etching, deep reactive ion etching (DRIE) process allows precise dimensional control with negligible undercuts and thus is preferred. DRIE also creates round corners that help evenly distribute the gaps between the die and the carrier. Based on experience, a cavity 10µm lager than the CMOS die on each side is ideal. After DRIE, 1µm thermal oxide is grown on the chip carrier to insulate the silicon substrate before subsequent metallization. Silicon carriers can be produced in batch using a whole wafer. The described lab-on-CMOS integration processes can also perform in wafer level.

A silicon chip carrier was prepared by etching a cavity through a 10mm square of silicon wafer, where the size of the cavity is 10µm lager than the CMOS die on each side. A DRIE process created straight side walls for precise dimension. DRIE also creates

rounded corners that allow leveling of the gaps between the die and the carrier. The etch rate using STS Pegsus DRIE tool was 0.3024 μm/s.

Dry-wet-dry thermal oxidation was performed to generate a silicon oxide coating over the carrier. The oxidation layer provided good electrical insulation in addition to polyimide. It is easy for water-based polyimide to be evenly distributed on hydrophilic silicon oxide instead of bare silicon.

5.3.3 Surface Leveling and Fixing

Surface leveling of the chip and carrier is critical for continuity of planar interconnects and microfluidic channels. To achieve micron-scale leveling, a unique process using wax was developed for the lab-on-CMOS platform. The chip carrier was place with its face down onto an Apiezon wax (M&I Materials, Manchester, UK) coated glass wafer. A CMOS chip was then placed faced down into the cavity of the carrier as shown as illustrated in Step 2 of Figure 5.1. The chip carrier and the chip were initially self-leveled by gravity. Before fixing the chip and carrier together, the wax was heated under vacuum to 150 ºC to reflow and to expel air bubbles. The reflowed wax further leveled the chip and carrier. The front of the chip and carrier were attached to wax at cooling down.

The thickness of the wax coating is critical to the success of integration. In order to control wax coating thickness, the Apiezon wax was diluted in xylene at 1:2, 1:4 and 1:8 and spun coated at 1000, 2000 and 3000rpm and. After the wax dried, its thickness was characterized using surface profiler. Plots in Figure 5.3 give the wax thickness as a function of spin speed and diluting ratio. In experiment trials, thinner coatings did not

provide adequate sealing; while thicker coating excessively extruded into the gap between chip and carrier. 2µm Apiezon wax coating was found appropriate. It was achieved by spin-on 1:2 Apiezon wax at 1000rpm.

After wax reflowing, epoxy was applied to fill the gap and to fix the CMOS chip to the carrier as shown in Figure 5.1 (Step 3). A thin glass cap was attached to the backside of the chip-carrier assembly to provide mechanical support to prevent carrier breakage along the sides of the cavity during subsequent handling. Although several fixing materials were explored, EPO-TEK 302-3M epoxy (Epoxy Technology, Billerica, MA) was chosen because Apiezon wax has low solubility in the solvent of the epoxy, so it does not mix the wax. Further, the expoxy resists to xylene and cholorobenzene used to remove wax. Low viscosity, low shrinkage and chemical are other desirable properties exhibited by this epoxy.

The chip-carrier assembly was released from the glass wafer by dissolving wax in xylene, and then cleaned using xylene, chlorobenzene, isopropyl alcohol and deionized water in sequence.

5.3.4 Planar Wiring

As shown in Fig. 5.3, because of wax flowing into the gap, a shallow trench was formed unfilled by the fixing material in the front side of the chip-carrier assembly. The depth of this trench is critical for successful electrical and fluidic interconnection across the gap and was controlled by controlling the wax thickness discussed previously.

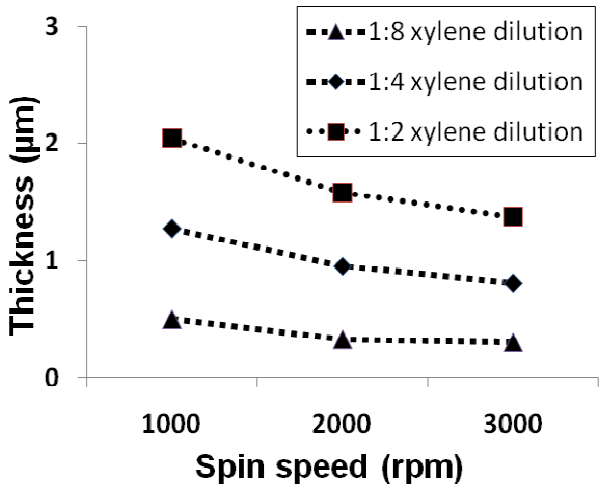

Figure 5.3: Spin-on Apiezon wax thickness as a function of spin speed and wax diluted in xylenes at 1:8, 1:4 and 1:2.

Although the trench depth can be minimized by careful selection of wax conditions, it cannot be eliminated. To fill this trench to create an even and continuous surface before metalization, a polyimide layer was applied, with the added advantage of smoothing the sharp edges of the silicon carrier and chip. PI 2554 polyimide precursor was obtained from HD MicroSystems (Parlin, NJ). A polyimide precursor diluted by its thinner at 1:1 was prepared, spun on the surface of the assembly and soft baked. S1813 photoresist was spun on, soft baked, exposed and developed. The base developer also etches off unmasked polyimide precursor. As shown in Step 4 of Fig. 5.1, the polyimide ring acts as a bridge over the trench providing an even and continuous surface for metallization. Characterization of the bridge structure is discussed in the Results section below.

Planar interconnects leading the CMOS chip pads to finger contacts at the edges of the carrier were formed using liftoff thin-film metals. Ti/Au (5nm/100nm) was deposited by thermal evaporation after photolithography. Tilted rotation during evaporation improves metal coverage on the slopes of the trenches and pad wells. Gold

electrodes (for electrochemical sensors) on the CMOS chip were formed at the same time as the interconnects, as shown in Step 5 of Figure 5.1.

5.3.5 Passivation and Planarization

Following metallization, a second polyimide layer was applied to insulate interconnects and form the bottom plane of the microfluidic structure, as illustrated in Step 6 of Figure 5.1. A thick polyimide layer was used to further planarize the surface. The polyimide was patterned as described in Section III.B to expose the on-CMOS electrodes and contact fingers at the edge of the carrier, as illustrated in Step 7 of Figure 5.1. A 500nm silicon dioxide layer was then deposited over polyimide by plasma enhanced chemical vapor deposition (PECVD) at 200 ºC and patterned using photolithography and HF wet etching. The oxide provides an adhesion layer for the PDMS fluidic structure and insulates the polyimide from the fluid channel. For a higher quality oxide, PECVD could be done at a higher temperature (~300 ºC); however, this would cure the polyimide and require alternative patterning tools such as O2/CF4 plasma dry etching or laser ablation.

5.3.6 Microfluidic Structure Integration

The final step in the lab-on-CMOS integration process was to attach the PDMS microfluidic structure to the chip-carrier assembly, as illustrated in Step 8 of Figure 5.1. The PDMS and the oxide surface were treated in oxygen plasma for enhanced bonding [6]. PDMS was chosen for the microfluidic structure because it permits electrode modification with sensitive materials, such as enzyme immobilization, before attachment of the microfluidic structure.

A fluidic structure of four mixers was designed in a 6mm by 10mm footprint, with the detection channels designed to run across the electrochemical sensors on the CMOS chip. An SU 8 master was created by photolithography using a transparency file photomask of the design. The channel height was 20µm, defined by the thickness of SU 8. Silane was vapor-primed on the master for easy peeling. Sylgard PDMS (Dow Corning, Midland, MI) was mixed and cured. The structure was cut out and released for use.

5.4 Result and Discussion

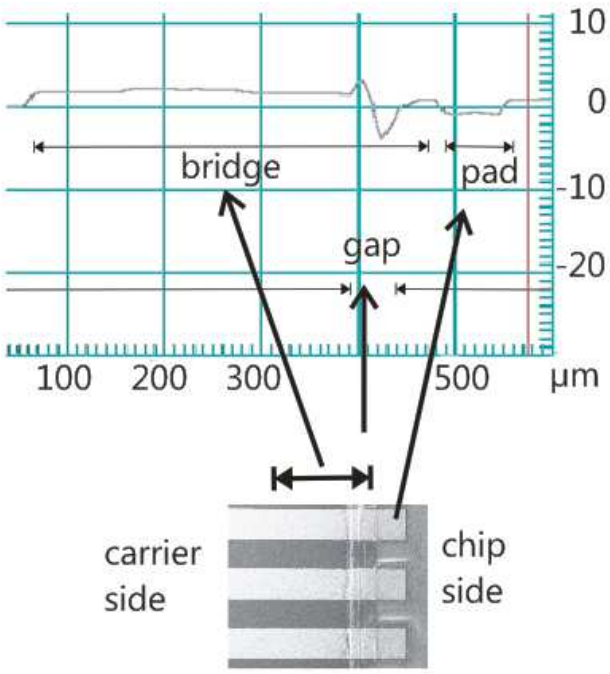

Figure 5.4: Surface profile from the carrier to the CMOS chip, measured before metallization, passivation and planarization. Bottom picture is a SEM image of interconnects over the bridge after metalization, to scale profilometer plot, confirming the continuity of metal traces routing the chip pads to the carrier perimeter over the gap via the bridge. Note: the horizontal axis scale is 10x the vertical scale. The zero position on the vertical axis is the elevation of the carrier.

A previously reported CMOS potentiostat chip [8] was prepared by gold plating bonding pads. A silicon chip carrier with a cavity matching the size of the potentiostat chip was fabricated using an STS Pegasus DRIE tool. The chip-carrier assembly was constructed using the integration process described by Figure 5.1.

The surface profile of the polyimide bridge between the CMOS chip and the carrier was characterized by a Dektak 3 surface profilometer, and is plotted in Figure 5.4. The plot shows shallow slopes were created by polyimide filling the gap and covering the sharp silicon edges. Notice that the x-axis is 10x scale of the y-axis and that the maximum slope along the surface is only 10º. The inset SEM image in Figure 5.4 confirms the metal traces were continuous over the trench. Using probe station, the interconnect resistance was measured from pads to finger contact to be 8.4±0.4Ω, as shown in Table 5.1. The current load capacity was over 500mA, sufficient for the CMOS

Measured	**Wire**	**Net (Ω)**
9.5	0.6	8.9
8.4	0.6	7.8
8.9	0.6	8.3
9	0.6	8.4
9.2	0.6	8.6
Average	8.4	
Std	0.4	

Table 5.1: Resistance from terminal to terminal (units: Ω).

potentiostat, as shown in Figure 5.5. Furthermore, the carrier and the CMOS chip were properly leveled, leaving the chip-carrier height difference of only 1µm as shown in the plot of Figure 5.4.

A 4-channel PDMS microfluidic mixer was constructed. The PDMS structure was treated under oxygen plasma and attached to the surface of the chip-carrier assembly, as shown in Figure 5.6. A toluidine blue-O solution was passed through the structure as shown without leakage. Electrical and fluidic characterization indicates successful integration of the lab-on-CMOS platform. The lab-on-CMOS device connected to a PCB interface board that allows on-CMOS electrochemical sensors to be tested in a microfluidic environment.

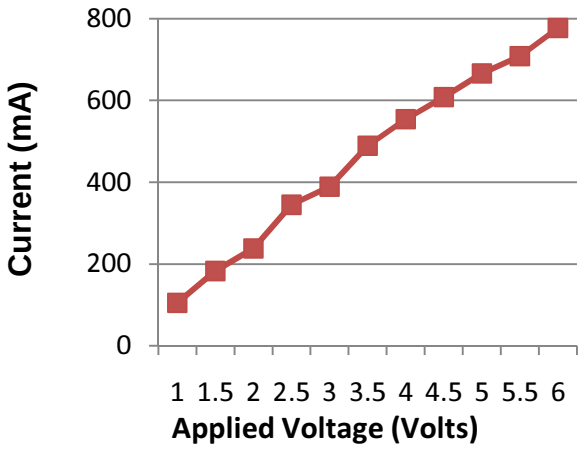

Figure 5.5: Current load test of planar wires.

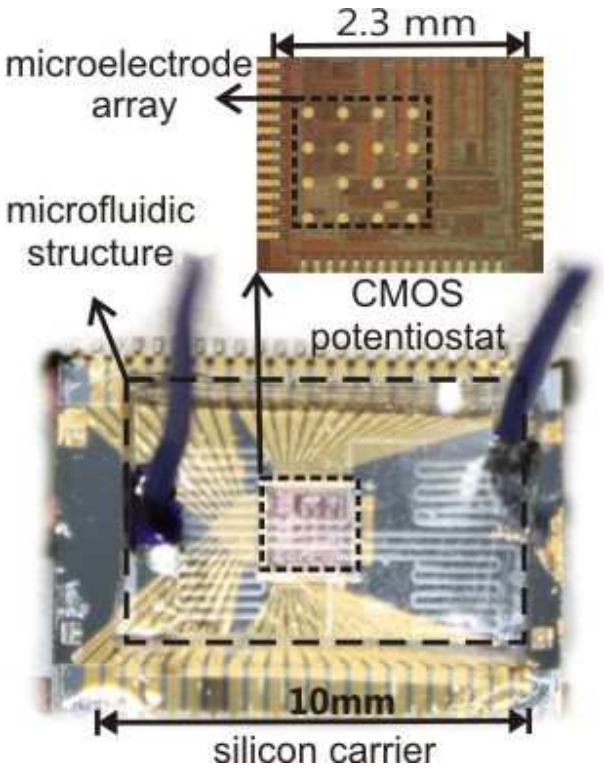

Figure 5.6: Surface profile from the carrier to the CMOS chip, measured before metallization, passivation and planarization. Inset is a SEM image of interconnects over the bridge after metalization, to scale profilometer plot, confirming the continuity of metal traces routing the chip pads to the carrier perimeter over the gap via the bridge. Note: the horizontal axis scale is 10x the vertical scale. The zero position on the vertical axis is the elevation of the carrier.

5.5 Conclusion

A new lab-on-CMOS platform for integrating microfluidics, on-CMOS electrode arrays, and CMOS electrochemical instrumentation chip was introduced. The fabrication process involving a CMOS die and a silicon chip carrier was described, and a prototype assembly was demonstrated. Electrical and fluidic characterizations verify successful integration of the lab-on-CMOS platform.

6 Summary, Contributions and Future Work

6.1 Summary

The mysteries of the vast unexplored world of biology have been motivating scientists to leverage micro/nanotechnology using lab-on-chip devices and microsystems. The power of microelectronics has not been adequately explored to enhance the signaling between biology and silicon. This thesis work introduces a lab-on-CMOS platform concept that enables integration of biosensors directly on top of a CMOS chip to establish continuous bio-to-silicon interaction pathways.

This research developed methodologies of optimizing the integration of redox enzyme-based electrochemical biosensor, microfabricated electrode and CMOS instrumentation with breakthroughs in those areas. The molecular self-assembly enzyme immobilization method was evaluated, leading to the development of a fabrication-favored method combining conductive polymers and molecular self-assembly. An miniaturized CMOS-compatible Ag/AgCl/PPy(Cl^-)/Nafion quasi-reference electrode was developed. A parallel bi-potentiostat architecture was developed replacing the traditional adder-potentiostat architecture to support redox recycling. An example fructose sensor was developed and the chronoamperometry technique was implemented through the CMOS bipotentiostat to extract analyte concentration without needs of further data processing. Finally, a unique CMOS die packaging scheme featuring a silicon chip carrier and microfabricated planar interconnections was developed to incorporate a microfluidic structure. The individual areas of contribution are summarized as below.

6.2 List of Contributions

a. *Introduced a methodology for integration of redox-enzyme-based biosensor arrays with a CMOS instrumentation chip*

This is the first known research into integration of an enzyme-based biosensor onto a CMOS electrochemical instrument chip using CMOS compatible electrode system. In order to minimize the footprint of an *Oxidoreductase* enzyme-based biosensor to fit on CMOS, redox recycling, a signal amplification mechanism was utilized to increase sensitivity, and a concentric ring electrode on CMOS chip surface. A CMOS bipotentiostat was developed for placement directly underneath the concentric ring electrode, enabling measurement using the chronoamperometry technique to extract the analyte concentration directly.

b. *Developed a novel CP-MSA technique to immobilize enzyme on aluminum*

A conductive polymer molecular self-assembly (CP-MSA) enzyme immobilization method was developed as an alternative to the MSA method for direct immobilization on CMOS aluminum without post-CMOS photolithography. With CP-MSA, the enzyme can be selectively immobilized on multiple working electrodes and does not foul the counter electrode like the alternative MSA process does. This method eliminates the dependence on gold and saves at least 50% processing time compared to MSA.

c. *Developed electrochemically optimized, CMOS compatible, planar electrode systems and fabrication processes*

Planar electrode systems were designed and fabricated to simultaneously establish optimized for 1) post-CMOS microfabrication, 2) biointerface quality and 3) electrochemical performance. For the first time, redox recycling on a concentric ring electrode was introduced to increase sensitivity and to reduce footprint of a redox-enzyme-based biosensor so that it can be implemented on CMOS. A CMOS-compatible Ag/AgCl/PPy(Cl^-)/Nafion quasi-reference electrode process was developed to enable down scaling and placement within a short distance from the working electrode, uniquely improving on-chip electrode density.

d. *Introduced a new bi-potentiostat architecture for effectively implementing onto CMOS*

A new bipotentiostat architecture was designed to support enzyme redox recycling through interdigitated electrodes. By replacing traditional adder-potentiostat architecture, the new architecture reduces circuit complexity and thus silicon area by 44% for each additional channel. The new architecture also completely avoids propagated potential control errors.

e. *Introduced a novel lab-on-CMOS package platform that enables high performance CMOS biosensor arrays to utilize complex microfluidics*

A lab-on-CMOS platform concept was introduced that provides an expanded area beyond the CMOS chip surface to allow integration of complex microfluidics. Through an innovative leveling process, a surface height difference between the CMOS chip and a silicon carrier of only 1µm was achieved. Microfabricated planar interconnection was

shown to successfully replace traditional bonding wires or solder bumps. Integrity of the microfluidic structures was verified through experimental measurement.

6.3 Future Work

This research has established the foundation for a lab-on-CMOS platform. Future full integration of enzyme-based biosensors on a CMOS bi-potentiostat would further demonstrate the power of combining microelectronics, microfabrication and biosensor technologies. To achieve this goal, the following works are crucial:

a. Enzyme biosensors on concentric-ring electrode

Using the mathematic model developed by this research, finite element analysis of concentric ring electrode can help predict current generated by the sensor. Electroless gold plating on the concentric ring electrode is required for using MSA method. Immobilization using CP-MSA method needs improvement on sensitivity and validation on CMOS aluminum concentric ring electrodes.

b. A self-contained CMOS electrochemical instrumentation

This research uses some off-chip auxiliary circuits and a DAQ. A self-contained CMOS bipotentiostat with digital control logic to interface with a wireless device will greatly enhance the optimization of biosensors, electrochemical instrumentation and electrochemical techniques as a system.

c. Characterization of on-chip planar electrodes in microfluidic channels

Off-chip biosensors were used for characterizing CMOS bipotentiostat in this research. On-chip biosensors using the concentric ring electrode can be characterized show its advantages over a disk electrode of the same area. Once packed in microfluidic channels, the performance of the on-chip electrodes can be characterized, with commercial potentiostat and then with the CMOS chip. An Ag/AgCl/PPy(Cl^-)/Nafion quasi-reference electrode can be fabricated on a CMOS chip.

d. Microfluidic integration

A suitable microfluidic structure such as mixing and separation could be designed and characterized to demonstrate the sample handling capability provided by the die-level lab-on-CMOS packaging scheme. More sophisticated passive or active microfluidic devices could be built on the chip carrier using silicon micro machining.

APPENDIX

Modeling of Redox Recycling on Concentric Ring Electrode

To characterize the concentric ring electrode, we consider that it is in a solution of species O. One working electrode, defined as generator electrode, is initially set at a potential where O is not reduced. The other electrode, defined as regenerator, is initially set to a potential where the reduction product *R* is oxidized. A step waveform is applied at $t = 0$, so that O is to reduced to *R* at the generator electrode; at the same time, another step waveform is applied on the regenerator electrode so that a portion of the reduced *R* transported onto generator can be oxidized to O. The concentration of O is increased by the regenerated O locally on the regenerator electrode. As a consequence, the regenerated O that diffused onto generator electrode increases the reduction current.

The diffusion of a planar electrode occurs in dimensions both normal to the electrode plane and radical with respect to the symmetrical axis. Consider the generator electrode in a cylindrical coordinate system, the diffusion equation is written as follows:

$$\frac{1}{D_o}\frac{\partial C_o(r,z,t)}{\partial t} = \frac{\partial^2 C_o(r,z,t)}{\partial r^2} + \frac{1}{r}\frac{\partial C_o(r,z,t)}{\partial r} + \frac{\partial^2 C_o(r,z,t)}{\partial z^2}$$

where r describes radial position normal to the axis of symmetry at $r = 0$, and *z* describes linear displacement normal to the plane of the electrode at $z = 0$, with D_0 for diffusion coefficient, C_0 for concentration at the electrode surface andt for time. Assuming the initial solution is homogenous, then concentration of O equals to the bulk concentration C_o^* all over the solution, including the electrode surface.

$$C_o(r, z, 0) = C_o^*$$

After the perturbation, the bulk concentration deep into the solution remains unchanged both radically and normal to the electrode plane.

$$\lim_{r \to \infty} C_o(r, z, t) = C_o^*$$

$$\lim_{z \to \infty} C_o(r, z, t) = C_o^*$$

If the k_{th} ring electrode is a generator electrode, then the adjacent $(k\text{-}1)_{th}$ and $(k+1)_{th}$ ring electrode is a generator electrode. In between the rings, there is no flux of C_o into or out of the mantle, since there is no reaction in the gap.

$$\frac{\partial C_o(r, z, t)}{\partial z} = 0$$

$$\left(r_k + {}^{d}/_{2} \leq r \leq r_{k+1} - {}^{d}/_{2} \; and \; r_{k-1} + {}^{d}/_{2} \leq r \leq r_k - {}^{d}/_{2} \right)$$

where r_k is the central radius of the k_{th} ring electrode, d is the width of the ring. The ring radius of the outer ring is larger than the inner ring by d, $r_{k+1} > r_k + d$, making sure the rings are not overlapped. Above conditions applies to the situation where the solution is homogenous before the perturbations and where the electrolyte extends beyond the

limit of the diffusion layer. After the experiment begins, we assume the concentration of O is driven to zero at the electrode surface:

$$C_o(r, 0, t) = 0, \qquad (r_k - {}^{d}/_{2} \le r \le r_k + {}^{d}/_{2}, t > 0)$$

Similarly, the diffusion equation of the regenerator electrode is:

$$\frac{1}{D_R}\frac{\partial C_R(r,z,t)}{\partial t} = \frac{\partial^2 C_R(r,z,t)}{\partial r^2} + \frac{1}{r}\frac{\partial C_R(r,z,t)}{\partial r} + \frac{\partial^2 C_R(r,z,t)}{\partial z^2}$$

Initial conditions of the regenerator electrodes are considered as follows. There is no R in presence at the beginning of the process all over the solution. The concentration of R equals to zero on the regenerator electrode surface as well as in the bulk solution.

$$C_R(r, z, 0) = 0$$

After the perturbation begins, the bulk concentration of R deep into the solution remains zero both radically and normal to the electrode plane.

$$\lim_{r\to\infty} C_R(r, z, t) = 0$$

$$\lim_{z\to\infty} C_R(r, z, t) = 0$$

As the nearby generator electrode, there is no flux of C_R into or out of the mantle in the gap between the $(k\text{-}1)_{th}$ regenerator and the k_{th} or $(k\text{-}2)_{th}$ generator electrode.

$$\frac{\partial C_R(r,z,t)}{\partial z} = 0$$

$$(r_{k-2} + {}^{d}/_{2} \le r \le r_{k-1} - {}^{d}/_{2} \; and \; r_{k-1} + {}^{d}/_{2} \le r \le r_k - {}^{d}/_{2})$$

where r_{k-1} is the radius at the center of the $k_{th\text{-}1}$ ring, a regenerator electrode, d is the width of the ring. After the experiment begins, we assume the concentration of *R* is driven to zero at the regenerator electrode surface:

$$C_R(r,0,t) = 0, \qquad (r_{k-1} - {}^{d}/_{2} \le r \le r_{k-1} + {}^{d}/_{2}, t > 0)$$

After the experiment begins, O is reduced to *R* at the k_{th} ring generator electrode and transports to the adjacent $(k\text{-}1)_{th}$ and $(k+1)_{th}$ regenerator electrodes. The reduction reaction starts with C_o^* , after the diffusion layer formed, is limited by mass transport. As a result, a wave of *R* is produced and then followed by a steady replenishing. If O is fully converted to *R* without any delay, the product concentration C_R approximately traces the

concentration of O right next to the electrode surface $z = \delta$ $(\delta \to 0)$, $C_O(r, \delta, t)$. This C_R adds to the boundary conditions of the diffusion equation of the regenerator electrode.

$$C_R(r, 0, t) \cong C_O(r, \delta, t)$$

$$(r_k - {}^{d}/_{2} \leq r \leq r_k + {}^{d}/_{2}, t > 0, \delta \to 0)$$

The generated *R* transports from k_{th} ring generator electrode to the adjacent $(k\text{-}1)_{th}$ and $(k+1)_{th}$ regenerator electrodes. Considering only diffusion portion of the mass transport, after a time delayt_d, it is re-oxidized on the regenerator electrodes.

$$t_d = (r_k - r_{k-1})^2/(2D_R)$$

The re-oxidized O carries the same temporal and spacial concentration profile as the *R* produced on the generator electrode, noted C_O^{reg}. On the regenerator electrode, the total concentration of O is C_O^{reg} adding to the existing O *in situ*.

$$C_O^{Total}(r, 0, t) = C_O(r, o, t) + C_O^{reg}(r, o, t)$$

$$(r_{k-1} - {}^{d}/_{2} \leq r \leq r_{k-1} + {}^{d}/_{2}, t > 0, \delta \to 0)$$

The increased C_O^{Total} updates the boundary condition of the diffusion equation of the generator electrodes, increasing the reduction current in a dynamic fashion due to the interaction of the generation and regeneration. The boundary condition of the outmost ring and innermost ring is a special case of the inner rings.

Due to the complexity of the problem, the analytical solution of the partial differential equation is not tempted. However, it is feasible to model the concentric ring electrode using finite element analysis program, and to derive the current-time relationship graphically by applying the boundary conditions discussed above.

REFERENCES

REFERENCES

[1] K. Rogers, "Biosensors for environmental monitoring: a regulatory perspective," *TrAC Trends in Analytical Chemistry*, vol. 14, pp. 289-294, 1995.

[2] M. Keusgen, "Biosensors: new approaches in drug discovery," *Naturwissenschaften*, vol. 89, pp. 433-444, 2002.

[3] J. Wang, "Amperometric biosensors for clinical and therapeutic drug monitoring: a review," *Journal of Pharmaceutical and Biomedical Analysis*, vol. 19, pp. 47-53, 1999.

[4] I. Moser, G. Jobst, and G. A. Urban, "Biosensor arrays for simultaneous measurement of glucose, lactate, glutamate, and glutamine," *Biosensors and Bioelectronics*, vol. 17, pp. 297-302, 2002.

[5] S. P. Mohanty and E. Kougianos, "Biosensors: a tutorial review," *Potentials, IEEE*, vol. 25, pp. 35-40, 2006.

[6] L. Clark and C. Lyons, "Electrode Systems for Continuous Monitoring in Cardiovascular Surgery," *Annals of the New York Academy of Sciences*, vol. 102, pp. 29-45, 1962.

[7] E.-H. Yoo and S.-Y. Lee, "Glucose Biosensors: An Overview of Use in Clinical Practice," *Sensors*, vol. 10, pp. 4558-4576, 2010.

[8] W. Schuhmann, C. Kranz, J. Huber, and H. Wohlschlager, "Conducting polymer-based amperometric enzyme electrodes. Towards the development of miniaturized reagentless biosensors," *Synthetic Metals*, vol. 61, pp. 31-35, 1993.

[9] M. Zayats, E. Katz, and I. Willner, "Electrical contacting of flavoenzymes and NAD(P)(+)-dependent enzymes by reconstitution and affinity interactions on phenylboronic acid monolayers associated with Au-electrodes," *Journal of the American Chemical Society*, vol. 124, pp. 14724-14735, 2002.

[10] B. L. Hassler, N. Kohli, J. G. Zeikus, I. Lee, and R. M. Worden, "Renewable dehydrogenase-based interfaces for bioelectronic applications," *Langmuir*, vol. 23, pp. 7127-7133, 2007.

[11] N. Ravindra, C. Prodan, S. Fnu, I. Padronl, and S. Sikha, "Advances in the manufacturing, types, and applications of biosensors," *JOM Journal of the Minerals, Metals and Materials Society*, vol. 59, pp. 37-43, 2007.

[12] M. Koudelka-Hep, "Microelectrode sensors for biomedical and environmental applications," *Electrochimica Acta*, vol. 45, pp. 2437-2441, 2000.

[13] R. M. Wightman, "Voltammetry with Microscopic Electrodes in New Domains," *Science*, vol. 240, pp. 415-420, 1988.

[14] Y. Huang, A. Mason, A. J. Greiner, R. Y. Ofoli, and R. M. Worden, "Post-CMOS Compatible Microfabrication of a Multi-Analyte Bioelectrochemical Sensor Array Microsystem," presented at 5th IEEE Int. Sensors Conf., Dageu, Korea, 2006.

[15] A. C. R. Grayson, R. S. Shawgo, A. M. Johnson, N. T. Flynn, Y. Li, M. J. Cima, and R. Langer, "A BioMEMS Review: MEMS Technology for Physiologically Integrated Devices," *Proceedings of the IEEE*, vol. 92, pp. 6-21, 2004.

[16] A. Frey, M. Schienle, C. Paulus, Z. Jun, F. Hofmann, P. Schindler-Bauer, B. Holzapfl, M. Atzesberger, G. Beer, M. Fritz, T. Haneder, H. C. Hanke, and R. Thewes, "A digital CMOS DNA chip," presented at Circuits and Systems, 2005. ISCAS 2005. IEEE International Symposium on, 2005.

[17] P. Levine, P. Gong, K. Shepard, and R. Levicky, "Active CMOS Array for Electrochemical Sensing of Biomolecules," San Jose, CA, USA, 2007.

[18] A. Manickam, A. Chevalier, M. McDermott, A. Ellington, and A. Hassibi, "A CMOS electrochemical impedance spectroscopy biosensor array for label-free biomolecular detection," presented at ISSCC, San Francisco, CA, USA, 2010.

[19] A. Hassibi and T. H. Lee, "A programmable electrochemical biosensor array in 0.18 μm standard CMOS," presented at Solid-State Circuits Conference, 2005. Digest of Technical Papers. ISSCC. 2005 IEEE International, San Francisco, CA, USA, 2005.

[20] P. Kruppa, A. Frey, I. Kuehne, M. Schienle, N. Persike, T. Kratzmueller, G. Hartwich, and D. Schmitt-Landsiedel, "A digital CMOS-based 24x16 sensor array platform for fully automatic electrochemical DNA detection," *Biosensors and Bioelectronics*, vol. 26, pp. 1414-1419, 2010.

[21] R. Reay, "Microfabricated electrochemical analysis system for heavy metal detection," *Sensors and Actuators B: Chemical*, vol. 34, pp. 450-455, 1996.

[22] D. Grieshaber, R. MacKenzie, J. V 枚 r 枚 s, and E. Reimhult, "Electrochemical Biosensors - Sensor Principles and Architectures," *Sensors*, vol. 8, pp. 1400-1458, 2008.

[23] Y. Wang, H. Xu, J. Zhang, and G. Li, "Electrochemical Sensors for Clinic Analysis," *Sensors*, vol. 8, pp. 2043-2081, 2008.

[24] N. Ronkainen, B. Halsall, and W. Heineman, "Electrochemical biosensors," *Chem. Soc. Rev.*, vol. 39, pp. 1747-1763, 2010.

[25] Y. Wu and S. Hu, "Biosensors based on direct electron transfer in redox proteins," *Microchimica Acta*, vol. 159, pp. 1-17, 2007.

[26] A. Bard and L. Faulkner, *Electrochemical Methods: Fundamentals and Applications*. New York: John Wiley & Sons, 2001.

[27] W. Shinwari, D. Zhitomirsky, I. Deen, P. R. Selvaganapathy, J. Deen, and D. Landheer, "Microfabricated Reference Electrodes and their Biosensing Applications," *Sensors*, vol. 10, pp. 1679-1715, 2010.

[28] I. Rubinstein, *Physical Electrochemistry: Principles, Methods and Applications*. New York: Marcel Dekker, 1995.

[29] S. Cosnier, "Biomolecule immobilization on electrode surfaces by entrapment or attachment to electrochemically polymerized films. A review," *Biosensors and Bioelectronics*, vol. 14, pp. 443-456, 1999.

[30] W. Schuhmann, "Conducting polymer based amperometric enzyme electrodes," *Microchimica Acta*, vol. 121, pp. 1-29, 1995.

[31] F. Kuechenmeister and E. Meusel, "Polypyrrole as an interlayer for bonding conductive adhesives to activated aluminum bond pads," *IEEE Transactions on Components, Packaging, and Manufacturing Technology: Part A*, vol. 20, pp. 9-14, 1997.

[32] G. G. Wallace, M. Smyth, and H. Zhao, "Conducting electroactive polymer-based biosensors," *TrAC Trends in Analytical Chemistry*, vol. 18, pp. 245-251, 1999.

[33] M. Gerard, A. Chaubey, and B. D. Malhotra, "Application of conducting polymers to biosensors," *Biosensors and Bioelectronics*, vol. 17, pp. 345-359, 2002.

[34] T. Ahuja, I. A. Mir, D. Kumar, and Rajesh, "Biomolecular immobilization on conducting polymers for biosensing applications," *Biomaterials*, vol. 28, pp. 791-805, 2007.

[35] C. Kranz, H. Wohlschlager, H.-L. Schmidt, and W. Schuhmann, "Controlled Electrochemical Preparation of Amperometric Biosensors Based on Conducting Polymer Multilayers," *Electroanalysis*, vol. 10, pp. 546-552, 1998.

[36] S. Cosnier, B. Galland, C. Gondran, and A. Le Pellec, "Electrogeneration of Biotinylated Functionalized Polypyrroles for the Simple Immobilization of Enzymes," *Electroanalysis*, vol. 10, pp. 808-813, 1998.

[37] W. Schuhmann, R. Lammert, B. Uhe, and H. L. Schmidt, "Polypyrrole, a new possibility for covalent binding of oxidoreductases to electrode surfaces as a

base for stable biosensors," *Sensors and Actuators B: Chemical*, vol. 1, pp. 537-541, 1990.

[38] B. Thompson, O. Winther-Jensen, J. Vongsvivut, B. Winther-Jensen, and D. MacFarlane, "Conducting Polymer Enzyme Alloys: Electromaterials Exhibiting Direct Electron Transfer," *Macromol. Rapid Commun.*, vol. 31, pp. 1293-1297.

[39] J. Rick and T.-C. Chou, "Using protein templates to direct the formation of thin-film polymer surfaces," *Biosensors and Bioelectronics*, vol. 22, pp. 544-549, 2006.

[40] J. Martins, S. Costa, M. Bazzaoui, G. Goncalves, E. Fortunato, and R. Martins, "Electrodeposition of polypyrrole on aluminium in aqueous tartaric solution," *Electrochimica Acta*, vol. 51, pp. 5802-5810, 2006.

[41] M. Bazzaoui, J. Martins, T. Reis, E. Bazzaoui, M. Nunes, and L. Martins, "Electrochemical synthesis of polypyrrole on ferrous and non-ferrous metals from sweet aqueous electrolytic medium," *Thin Solid Films*, vol. 485, pp. 155-159, 2005.

[42] J. Voldman, M. Gray, and M. Schmidt, "Microfabrication in Biology and Medicine," *Annual Review of Biomedical Engineering*, vol. 1, pp. 401-425, 1999.

[43] H. Suzuki, "Advances in the Microfabrication of Electrochemical Sensors and Systems," *Electroanalysis*, vol. 12, pp. 703-715, 2000.

[44] S. Hwang, C. LaFratta, V. Agarwal, X. Yu, D. Walt, and S. Sonkusale, "CMOS Microelectrode Array for Electrochemical Lab-on-a-Chip Applications," *Sensors Journal, IEEE*, vol. 9, pp. 609-615, 2009.

[45] B. Polk, A. Stelzenmuller, G. Mijares, W. MacCrehan, and M. Gaitan, "Ag/AgCl microelectrodes with improved stability for microfluidics," *Sensors and Actuators B: Chemical*, vol. 114, pp. 239-247, 2006.

[46] S.-I. Park, S. Jun, S. Park, H. Kim, and S. Kim, "Application of a new Cl-plasma-treated Ag/AgCl reference electrode to micromachined glucose sensor," *IEEE Sensors Journal*, vol. 3, pp. 267-273, 2003.

[47] G. Valdesramirez, G. Alvarezromero, C. Galanvidal, P. Hernandezrodriguez, and M. Ramirezsilva, "Composites: A novel alternative to construct solid state Ag/AgCl reference electrodes," *Sensors and Actuators B: Chemical*, vol. 110, pp. 264-270, 2005.

[48] D. J. G. Ives and G. J. Janz, *Reference Electrodes, Theory and Practice (1st edition)*: Academic Press, 1961.

[49] M. Kimura, H. Fukushima, Y. Sagawa, K. Setsu, H. Hara, and S. Inoue, "An Integrated Potentiostat With an Electrochemical Cell Using Thin-Film Transistors," *IEEE Transactions on Electron Devices*, vol. 56, pp. 2114-2119, 2009.

[50] J. Ghilane, P. Hapiot, and A. J. Bard, "Metal/Polypyrrole Quasi-Reference Electrode for Voltammetry in Nonaqueous and Aqueous Solutions," *Anal. Chem.*, vol. 78, pp. 6868-6872, 2006.

[51] M. Nolan, S. Tan, and S. Kounaves, "Fabrication and Characterization of a Solid State Reference Electrode for Electroanalysis of Natural Waters with Ultramicroelectrodes," *Analytical Chemistry*, vol. 69, pp. 1244-1247, 1997.

[52] L. Tymecki, E. Zwierkowska, and R. Koncki, "Screen-printed reference electrodes for potentiometric measurements," *Analytica Chimica Acta*, vol. 526, pp. 3-11, 2004.

[53] H. Suzuki, A. Hiratsuka, S. Sasaki, and I. Karube, "Problems associated with the thin-film Ag/AgCl reference electrode and a novel structure with improved durability," *Sensors and Actuators B: Chemical*, vol. 46, pp. 104-113, 1998.

[54] S. Ayers, K. Gillis, M. Lindau, and B. Minch, "Design of a CMOS Potentiostat Circuit for Electrochemical Detector Arrays," *IEEE transactions on circuits and systems. I, Regular papers : a publication of the IEEE Circuits and Systems Society*, vol. 54, pp. 736-744, 2007.

[55] F. Yalcinkaya, "Ag/AgCl/Cl^- coated silver-stripe reference electrode," *Medical Engineering & Physics*, vol. 19, pp. 299-301, 1997.

[56] R. Zielinska, "All-solid-state planar miniature ion-selective chloride electrode," *Analytica Chimica Acta*, vol. 451, pp. 243-249, 2002.

[57] W.-Y. Liao and T.-C. Chou, "Fabrication of a Planar-Form Screen-Printed Solid Electrolyte Modified Ag/AgCl Reference Electrode for Application in a Potentiometric Biosensor," *Analytical Chemistry*, vol. 78, pp. 4219-4223, 2006.

[58] K.-S. Yun, H.-J. Kim, S. Joo, J. Kwak, and E. Yoon, "Analysis of heavy-metal-ions using mercury microelectrodes and a solid-state reference electrode fabricated on a Si wafer," Tokyo, Japan, 2000.

[59] K. Nagy, K. Eine, K. Syverud, and O. Aune, "Promising New Solid-State Reference Electrode," *Journal of The Electrochemical Society*, vol. 144, pp. L1-L2, 1997.

[60] F. Moussy and J. Harrison, "Prevention of the Rapid Degradation of Subcutaneously Implanted Ag/AgCl Reference Electrodes Using Polymer Coatings," *Analytical Chemistry*, vol. 66, pp. 674-679, 1994.

[61] N.-H. Kwon, K.-S. Lee, M.-S. Won, and Y.-B. Shim, "An all-solid-state reference electrode based on the layer-by-layer polymer coating," *Analyst*, vol. 132, pp. 906-912, 2007.

[62] A. Gore, S. Chakrabartty, S. Pal, and E. C. Alocilja, "A Multichannel Femtoampere-Sensitivity Potentiostat Array for Biosensing Applications," *Circuits and Systems I: Regular Papers, IEEE Transactions on [Circuits and Systems I: Fundamental Theory and Applications, IEEE Transactions on]*, vol. 53, pp. 2357-2363, 2006.

[63] S. M. Martin, F. H. Gebara, T. D. Strong, and R. B. Brown, "A low-voltage, chemical sensor interface for systems-on-chip: the fully-differential potentiostat," presented at Circuits and Systems, 2004. ISCAS '04. Proceedings of the 2004 International Symposium on, 2004.

[64] X. Zhu and C. H. Ahn, "On-Chip Electrochemical Analysis System Using Nanoelectrodes and Bioelectronic CMOS Chip," *Sensors Journal, IEEE*, vol. 6, pp. 1280-1286, 2006.

[65] K. Murari, M. Stanacevic, G. Cauwenberghs, and N. V. Thakor, "Integrated potentiostat for neurotransmitter sensing," *IEEE Engineering in Medicine and Biology Magazine*, vol. 24, pp. 23-29, 2005.

[66] W.-S. Wang, W.-T. Kuo, H.-Y. Huang, and C.-H. Luo, "Wide Dynamic Range CMOS Potentiostat for Amperometric Chemical Sensor," *Sensors*, vol. 10, pp. 1782-1797, 2010.

[67] L. Busoni, M. Carlà, and L. Lanzi, "A comparison between potentiostatic circuits with grounded work or auxiliary electrode," *Review of Scientific Instruments*, vol. 73, pp. 1921, 2002.

[68] O. Niwa and M. Morita, "Carbon Film-Based Interdigitated Ring Array Electrodes as Detectors in Radial Flow Cells," *Analytical Chemistry*, vol. 68, pp. 355-359, 1996.

[69] D. Farina and C. Cescon, "Concentric-ring electrode systems for noninvasive detection of single motor unit activity," *IEEE Transactions on Biomedical Engineering*, vol. 48, pp. 1326-1334, 2001.

[70] S. Sze, *Semiconductor Devices: Physics and Technology, 2nd Edition*. New York: John Wiley & Sons, 2002.

[71] R. F. Pierret, *Semiconductor Device Fundamentals*: Addison-Wiley, 1995.

[72] K. C. Tang, E. Liao, W. L. Ong, J. D. S. Wong, A. Agarwal, R. Nagarajan, and L. Yobas, "Evaluation of bonding between oxygen plasma treated polydimethyl siloxane and passivated silicon," *Journal of Physics: Conference Series*, vol. 34, pp. 155, 2006.

[73] A. Strandjord, S. Popelar, and C. Jauernig, "Interconnecting to aluminum- and copper-based semiconductors (electroless-nickel/gold for solder bumping and wire bonding)," *Microelectronics Reliability*, vol. 42, pp. 265-283, 2002.